On-tubing fluorescence measurements of the band broadening of contemporary injectors in ultra-high performance liquid chromatography

Broeckhoven, Ken; Vanderlinden, Kim; Guillarme, Davy; Desmet, Gert

Published in:
Journal of Chromatography A

DOI:
10.1016/j.chroma.2017.12.032

Publication date:
2018

Highlights:

- Localized measurements of injector band broadening are obtained using on-tubing fluorescence detection
- A distinction between the volumetric and the hydrodynamic contribution could be made
- Flow-through needle injection is compared with fixed loop injection
- Parameter values frequently used in literature to estimate $\sigma^2_{V,inj}$ from V_{inj} can lead to grave underestimation of $\sigma^2_{V,inj}$

On-tubing fluorescence measurements of the band broadening of contemporary injectors in ultra-high performance liquid chromatography

Ken Broeckhoven[1,*], Kim Vanderlinden[1], Davy Guillarme[2], Gert Desmet[1]

[1] Department of Chemical Engineering, Vrije Universiteit Brussel, Pleinlaan 2, 1050 Brussels, Belgium
[2] School of Pharmaceutical Sciences, University of Geneva, University of Lausanne, CMU - Rue Michel Servet 1, 1211 Geneva 4, Switzerland

*Corresponding author: Phone: (+)32.(0)2.629.37.81, Fax: (+)32.(0)2.629.32.48, e-mail: kbroeckh@vub.ac.be

Abstract

We report on a detailed study of the injection contribution to band broadening in contemporary UHPLC-instruments, using either flow-through needle or fixed loop injection (full loop). Using on-tubing fluorescence measurements at the outlet of the injector valve, very localized and undisturbed measurements were obtained. Varying both the flow rate and the injected volume allowed to split the injection variance ($\sigma^2_{V,inj}$) in a volumetric component (related to the amount injected) and a hydrodynamic component (related to the flow rate). For the flow-through needle injector and for the small injection volumes (< 2µL) typically used in UHPLC, it was found that the volumetric contribution (i.e. the part of $\sigma^2_{V,inj,}$ that increases with increasing injection volume) is given by a value of $\sigma^2_{V,inj,vol}$=0.8 to 1·V_{inj}^2 rather than by the value of 0.125 to 0.2·V_{inj}^2 that is normally assumed in literature. For the hydrodynamic contribution to $\sigma^2_{V,inj,}$ (i..e, the part which remains present even for very small injection volumes), a clear increase in dispersion with flow rate is found, reaching a plateau around 0.8ml/min of 0.6µL² or 1.2µL² for the 75µm and 120µm needle seat capillaries respectively. The difference between both shows the clear advantage of using a low dispersion 75µm injection needle seat capillary. For a loop-type injector operated in a full-loop mode, the increase in peak variance with the injection volume is much less pronounced, leading to a total injector variance given by $\sigma^2_{V,inj}$= 0.34µL²+0.12.V_{inj}^2 over the entire range of investigated injection volumes of 1.1µL up to 4.5µL when using 120µm or narrower ID loops. This expression was nearly completely independent of the flow rate. For larger ID sample loops, a clear increase of peak variance with flow rate at fixed injection volume was observed ($\sigma^2_{V,inj}$ increases with 20% for a 170µm ID loop and with 70% for a 220µm ID loop from 0.3 to 1ml/min).

1. Introduction

In recent years, a large number of studies have been undertaken to characterize the dispersion taking place in the fluidic connections of commercial ultra-high performance chromatographic instruments [1-22], since it contributes significantly to the total band broadening when using short, narrow inner diameter (ID) columns packed with sub-3µm particles. In general, the extra-column contribution is measured by replacing the column with a zero-dead volume (ZDV) connection [7-16] or by extrapolating the volumetric dispersion $\sigma_{V,tot}^2$ for a homologous series of compounds with increasing retention towards $(1+k)^2 = 0$ [17-22]. Most studies only focus on the combined contribution of the different parts of the chromatographic system (injector, connection tubing, preheaters, valves, detector), because they only need the total extra-column dispersion to correct the measured total dispersion to determine the "column-only" band broadening. Some studies went a step further and attempted to separate the effect of pre- and post-column contributions, or the effects of individual aspects, such as injection volume [1,3,4,12,23,24]. Understanding extra-column band broadening and, more specifically, the variance contribution of injector valves and sample loops is also critical for the design of improved multi-dimensional LC systems [25,26]. In most cases, the different contributions to band broadening are considered to be independent and additive and the total peak variance in volumetric units is usually written as [1,4,8,9,11,12,16-19,21,23]:

$$\sigma_{V,tot}^2 = \sigma_{V,pre}^2 + \sigma_{V,col}^2 + \sigma_{V,post}^2 \quad (1)$$

with the subscript 'col' corresponding to the column variance, and 'pre' and 'post' representing the fluidic path before (injector to column inlet) and after the column (from column outlet up to and including detector cell) respectively. Using the ZDV method, it is assumed the extra-column variance given by Eq. (1) with $\sigma_{V,col}^2 = 0$. However, the assumption that the pre and post column contributions are additive is not entirely true. This is due to the fact that, for the typical combinations of tubing length, ID and flow rates used in (U)HPLC, the dispersion in the inlet tubing has not reached its long time limit yet when it reaches the ZDV connector, whereas the additivity of variances only holds for systems in their long time dispersion limit [5,27-28]. A recent study indicates that, for this reason, the ZDV method overestimates the extra-column dispersion contribution by about 1.5µL² on a total system contribution of 2.5µL² [5].

Both the pre- and post-column contributions can be further subdivided into different parts, distinguishing the different pieces of connection tubing, the injection volume and the injector valve, preheaters or post-column coolers (e.g. for high temperature LC) and the detector cell. For the pre-column train, this subdivision can be written as [9,12,23]:

$$\sigma_{V,pre}^2 = \sigma_{V,inj}^2 + \sigma_{V,tub,pre}^2 \quad (2)$$

wherein $\sigma_{V,tub,pre}^2$, is the combined effect of the hydraulic circuitry connecting the injector valve to the column, which in the presence of a pre-column heat-exchanger, consists of different pieces of tubing, connectors, as well as of the internal channel leading through the heat exchanger.

In the present study, we only focus on the very first contribution in Eq. (2), i.e., on the variance of the bands produced by the injector ($\sigma_{V^2,inj}$), prior to entering the pre-column tubing. In a practical way, this value can be split up in two parts. First, one has the peak variance that persists when the volume is decreased to almost zero, because the sample anyhow has to pass through the groove and bores of the injection valve (and also through the needle seat and tubing in case of a flow-through injector). This contribution is always present, even if only an infinitely thin slice of sample would be injected and is further referred to as the "hydrodynamic contribution", $\sigma_{V^2,inj,hydro}$. Secondly, one has a contribution that becomes increasingly larger with increasing injection volume, referred to here as the "volumetric contribution", $\sigma_{V^2,inj,vol}$.. Together, both can be added to yield:

$$\sigma^2_{V,inj} = \sigma^2_{V,inj.vol}(V_{inj}) + \sigma^2_{V,inj.hydro} \quad (3)$$

Although Eq. (3) is helpful in a practical sense, it should be realized both contributions are difficult to separate completely, as the volumetric part in practice inevitably also always depends on the flow rate, while the length of the hydrodynamic tract (and hence the hydrodynamic injector dispersion) also depends on the injection volume. It is thus important to note that $\sigma_{V^2,inj,vol}$ will hence also include a hydrodynamic contribution. Nevertheless, Eq. (3) still provides a convenient representation of the minimal amount of hydrodynamic dispersion all injected peaks have been subjected to ($\sigma_{V^2,inj,hydro}$) as well as of the variance contribution that increases with increasing injection volume ($\sigma_{V^2,inj,vol}$). A similar differentiation between those two contributions was made by Claessens *et al.* when investigating injection systems for open-tubular liquid chromatography [29], for normal and narrow bore column HPLC by Coq *et al.* Coq [30] and Sanchez *et al.* [31].

The "V_{inj}" between the brackets in Eq. (3) has thus been added to emphasize that we explicitly define $\sigma_{V^2,inj.vol}$ here as the part of the injection band broadening that varies with V_{inj}, and can hence be eliminated by injecting ever smaller and smaller injection volumes.

The dispersion volumetric contribution ($\sigma_{V^2,inj.vol}$) is generally related to the square of the injection volume via a dummy factor $1/\theta_{inj}$ [1,3,7,9,12,16,17,23,29,32-34] (also denoted as $1/D^2$, $1/K^2$, $1/k^2$).

$$\sigma^2_{V,inj.vol} = \frac{V^2_{inj}}{\theta_{inj}} \quad (4)$$

Ideally, i.e., if a perfectly rectangular injection band could be injected, this factor would be equal to 1/12 (variance of a rectangular plug), whereas a perfect mixer (without dead zones) yields a value of $1/\theta_{inj}=1$ [7,9,29,30,32,34-37]. In most literature, a range of $1/8<1/\theta_{inj}<1/5$ is proposed [30-32,34,37]. In practice, however, a much wider variety of $1/\theta_{inj}$-values has been reported, ranging from 1/12 over 1 [12,17,23,30,32,34,35,38] to even 50 [38]. In part, the wide variation in reported $1/\theta_{inj}$-values in literature may be explained by the fact that the distinction between $\sigma_{V^2,inj.vol}$ (for which the $1/\theta_{inj}$-factor has been originally introduced) and $\sigma_{V^2,inj}$ is not always made. Another

reason for the wide range of reported values is that the dispersion also depends on the type of injector, i.e. can be expected to be different for a full loop, a partial loop or a flow-through needle injector.

An alternative method to represent $\sigma_{V^2,inj}$ instead of Eq. (3) would be to assume that the injection variance always has a minimum value of $V_{inj}^2/12$ (i.e., the variance of a perfectly rectangular plug) and to treat all additional dispersion caused by the non-equilibrium dispersion as hydrodynamic dispersion. This would however depend on both the operating flow rate and injection volume, making the discussion of the effect of V_{inj} on $\sigma_{V^2,inj}$ cumbersome.

In the present study, we measured $\sigma_{V^2,inj}$ and its constituent contributions for a number of state-of-the art injection systems using an on-capillary LED-Light Induced Fluorescence detector (abbreviated as LIF in this work), offering the unique possibility to measure the dispersion as close as to the injector as possible (in practice, typically around 5-10cm away from the valve port). Varying the injection volume, it was also attempted to study the two different contributions to Eq. (3) separately. Only the flow-through needle and the full loop injection mode were considered. The flow-through needle injector consists of a sample needle which is moved into the sample vial to load the sample into the needle and the sample loop connected to it, according to the FILO principle (First in Last out) [39]. Subsequently they are placed back in line via a needle-seat connection in which the needle is pushed to seal against the operation pressure. After a valve switch, the loop and needle are placed back in line and the sample is injected by eluting from the needle, through the needle seat and needle seat capillary and the injector valve. For a fixed loop injector, the sample is first drawn into a needle (with loop) and subsequently this is injected in a sample loop. It is required to draw a larger volume than the sample loop volume to compensate for the volume of the flow path between needle and loop and to ensure full filling of the loop (in full loop mode this requires at least 2 times the loop volume) [39]. The loop is directly connected to the valve and the sample plug therefore does not need to travel through an additional capillary (see Fig. 1).

Partial loop injections are more complex and are hence more difficult to systematically investigate and model. This is due to the fact that most instruments also introduce a small air bubble in the loop before and/or after the sample to optimize the delivered sample plug, but technical aspects of this methodology vary from one vendor to the other. Another reason why the partial loop method was left outside the scope of the study is that it can be assumed to display a behavior that is intermediate between that of a fixed loop and a flow-through needle injector. In fact, if the loop is considered to be equivalent to the needle, the only difference between a partial loop and flow-through needle injection is the (much) shorter flow path of the former, because of the absence of the needle seat and needle seat capillary, eliminating to a large extent the contribution of $\sigma_{V^2,inj,hydro}$. The difference in effective flow path between the fixed loop and the flow-through injector is visualized in Fig. 1 using the dashed arrowed line geometrically defining the injector contribution as measured in the present study.

2. Materials and Methods

2.1 Instrumentation

Different chromatographic systems were used for the measurements. The main system (System 1) was an Agilent LC 1290 Infinity II (Agilent technologies, Waldbronn, Germany) with a binary pump (G7120A) and an autosampler (G7167D). The autosampler was equipped with the dual-needle option that results in two flow paths with two needles, the sample loops and needle-seats, along with an additional valve. The important aspect of this autosampler for the current investigation is that the sample is pressurized before injection, yielding practically no pressure dip upon injection due to the re-pressurization of the sample loop and needle. Two different needle seats with different needle seat capillary were used, i.e. with a 120µm ID (G4267-87012) and with a 75µm ID (G4267-87020), both 15cm long. A second system (System 2) was an Agilent LC 1290 Infinity with a quaternary pump (G4204A), a standard autosampler (i.e., with a single needle, G4226A). The third system (System 3) was an Agilent LC 1290 Infinity equipped with a binary pump (G4220A), but using a SFC multisampler (G4303A) in full-loop mode and a SFC Fusion A5 module (G4301A) to handle the wash steps of the sampler. Systems 1-3 were coupled using a Universal Interface Box (UIB, G1390B) to interface with the LED-Light Induced Fluorescence detector (ZETALIF LED 480) from Picometrics (Picometrics Technologies SAS, Labège, France). Finally, an Acquity I-class Ultra Performance Liquid Chromatography system from Waters (Milford, MA, USA) was used (System 4). This instrument was equipped with a binary solvent pump, an autosampler with a flow-through needle (FTN) injection system and a column oven set at 40°C and a UV detector. For Systems 1-3, data acquisition, data handling and instrument control were performed by Agilent Chemstation, for System 4 by Empower Pro 2 (Waters, Milford, MA, USA) software.

2.2 Experimental conditions

All experiments with the LIF were performed using pure methanol (Biosolve, Valkenswaard, The Netherlands) as the mobile phase and sample solvent, to prevent peak distortion due to solvatochromic shifts [40]. Coumarin 480 (also known as Coumarin 102) was used as the fluorescent dye (Sigma-Aldrich, Overijse, Belgium). Typically, the coumarin was dissolved in methanol at a concentration of 500µg/mL for the flow-through needle experiments and 200µg/mL for the full loop injections. The LIF was equipped with a 480nm LED source and a standard emission filter block (515-760nm). The photomultiplier high voltage was set to 700V and the rise time to 0.01s. The sampling rate (determined by the UIB) was set to 100Hz with a response time of <0.031s. Poly-imide coated fused silica capillaries with an ID of 50 and 200µm were purchased from Polymicro Technologies (Phoenix, Arizona, USA). To obtain a detection window for the LIF, the coating was burned off over a distance of 3mm after which the capillary was placed in the detection cell holder. The resulting 'detection cell' thus had a volume of around 6nL (50µm ID) and as a result had a negligible contribution to the measured dispersion. To keep the cell

in place near the injector valve, an arm holder for LIF-LC coupling (12-80CEL/LC) was used. Care had to be taken not to shift the cell or capillary during the experiments as displacement of the optical window can lead to loss in signal and an increase in noise when the window is no longer aligned in the detection cell.

For the experiments with the retained compounds using a UV detector, water was obtained from a MilliQ Purification System from Millipore (Bedford, MA, USA) and acetonitrile (gradient grade), methyl- and ethylparaben were purchased from Sigma–Aldrich (Buchs, Switzerland). The sample compounds were dissolved at a concentration of 100µg/ml in the same solvent composition (50/50 v%/v% ACN/H_2O) as the mobile phase. The column used for these experiments was an Xbridge BEH C18 2.5µm 2.1x100mm XP column. The UV detector operated with a 500nL flow cell, set to 254nm and a 80Hz sampling rate.

2.3 Experimental set-up and configuration

Fig. 1 schematically illustrates the different experimental set-up used in the investigation. Fig. 1a shows the standard flow-through needle design, with the needle seat and connection capillary to the injection valve. For the experiments with the Infinity II system (System 1), the actual valve and rotor configuration is more complex as the dual needle option was installed, but the added complexity is not shown in Fig. 1a as it does not result in any practical difference in the injection flow path from the sample to the detector. As two different needle seats were used, the 15cm connection capillary from the needle seat to the injection valve had either a 75µm or 120µm ID. For the experiments on the Infinity I (System 2), only the 75µm ID version was tested (10cm long). In one case (see Section 3.2) the length of capillary between the valve and the LIF detector was much larger (80cm) than presented in Fig. 1a, but usually this was about 8cm. Fig. 1b shows the set-up for the fixed loop injector, where the sample only needs to be flushed from the loop through the rotor and port of the injection valve towards the capillary.

3. Results and Discussion

3.1 Comparison of the injected peak shapes obtained with the different injector types

Fig. 2a represents the shapes of the injection peaks plugs obtained by injecting different volumes via the flow-through needle injector of System 1 (equipped with the 75µm ID needle seat), as recorded immediately after the injection valve on the 50µm fused silica capillary. It can clearly be seen that the peak height increases and the location of the apex shifts to higher elution times with increasing injection volume. For the largest injection volume, the signal reaches a plateau (which was checked not to be due to detector overloading), as the sample band loaded in the needle becomes so wide that only the front and the back end of the band were affected by the dispersion [9,30,38]. The injected bands were also clearly not Gaussian. Their variance can hence not be simply determined via the peak width at half height. The moment of methods would be the theoretically correct approach, but since the peaks exhibit a rather long, but very shallow tail, the resulting moment values are so large (i.e., are so strongly influenced by the tail) that they only have a limited practical relevance [6]. As a compromise, all variances were based on the peak width at 4.4% of the peak height, assuming this width is equal to 5σ (5σ-peak width method). In parallel, the data was also processed using the method of moments and the most relevant results of this study using this method are reported and discussed in the Supplementary Material.

Figs. 2b-c show the equivalent measurements for the different fixed loop injector configurations explored on System 3. Fig. 2b shows the effect of the length of the different considered 120µm ID loops, while Fig. 2c shows the other ID loops. Overlaid on Fig. 2c are two loops with a 120µm ID that have a similar volume (see Table 1) as the 220µm and 170µm loops (cf. dashed curves with corresponding colours). Two clear observations can be made from these figures. Firstly, the peaks are significantly narrower for the full loop injections than for the flow-through needle case (compare x-axis with Fig. 2a). Secondly, the peaks in the full loop mode reach a plateau (i.e., adopt a shape that is getting closer to a perfect rectangle) at much lower injection volumes than in the flow-through needle injector. E.g., the 2.7µL fixed loop injection already produces a clear flat top, while this only occurs for injection volumes on the order of 10µL or more in the flow-through needle case.

Considering the two largest loops (120µm, 28cm, black dashed curve, and 220µm, 10cm, full gray curve) it is clear that the peak for the latter is narrower, which is in agreement with the 25% smaller volume (4.5µL vs. 3.6µL), but exhibits a more pronounced tail. A similar, observation can be made for the 120µm (1.7µL, dashed red curve) vs. the 170µm loop (2.0µL, full orange curve), but less pronounced due to the smaller difference in loop ID. It thus appears that narrower ID loops result in more rectangular shaped injection bands in full loop injection mode. In addition, the peak variance increases more significantly with flow rate for the large ID loop, as will be discussed in detail in Section 3.5. This more pronounced tailing for large ID and flow rate dependency is in agreement with the results of Prüß *et al.* and Foster *et al.* [33,38], who showed more pronounced tailing when larger ID's were used for loop type injectors. The downside of narrower ID loops is however the very strong increase in pressure drop (pressure drop ~1/diameter^6 for a given fixed loop volume!).

3.2 Volumetric contribution to band broadening for flow-through needle injector measured via on-tubing LIF

Fig. 3a shows how $\sigma^2_{V,inj}$ (5σ-height based, see SM for moment based values) increases as a function of V_{inj}^2 in the flow-through needle injector of System 1 at a flow rate of 0.7ml/min. Injected volumes ranged from 0.1µL to 10µL (i.e. for a range of V_{inj}^2 of 4 orders of magnitude). All measurements were carried out with sample loop pre-compression and the peak variance of an ideal rectangular plug (θ=12) is added in this and subsequent figures as a dashed line. Three different configurations were considered to investigate the effect of the needle seat capillary and to validate the experimental methodology to isolate the volumetric contribution. First, two different needle seat capillaries (both 15cm) of 120µm (diamonds) and 75µm (circles) ID were tested with the LIF placed on a 50µm fused silica capillary, with the detection window right behind the injector valve, subsequently the 120µmID needle seat was also tested with the LIF detector placed at the end of a 80cm long, 200µm ID capillary (triangles). As expected, due to the dispersion contribution in the wide and long capillary, the observed values for the latter were shifted upward. However, the relation to the injection volume was in all three cases very similar, showing a fast initial increase of σ_V^2 which then levels off and further increases in an almost linear way, as indicated by the dotted lines on Fig. 3a (for V_{inj}>2.5µL, R^2>0.99 and V_{inj}>5µL, R^2>0.999 were found for linear fits). When zooming in on the small injection volumes (for V_{inj} < 1.5µL or V_{inj}^2 < 2.25µL², see Fig. 3b), a similar quasi-linear trend can be observed (albeit with a much higher slope). Although all measurement conditions were identical, a difference in dispersion of around 0.4-0.5µL² was found between the 120µm and 75µm needle seat capillaries for low injection volumes. For the very small injection volumes (and corresponding small signals) some scatter was observed but in general the results have a very good repeatability (each measurement of a triplicate repeat was plotted separately and not the average of the three subsequent ones). For volumes <0.25µL the data are bunched up rather closely, as the contribution from the injection volume itself becomes so small that it becomes negligible compared to that from the dispersion in the needle seat, tubing and injector valve. To check the linearity of the LIF detection, the peak areas were determined and found to linearly increase with the injection volume (R^2=0.9998) over the entire range of injection volumes.

As already mentioned, it can be expected that the contribution from the volume itself ($\sigma^2_{V,inj.,vol}$) becomes negligible for very small injection volumes ($V_{inj} \approx 0$) compared to the hydrodynamic part ($\sigma^2_{V,inj.hydro}$) (see Eqs. (3)-(4)). Therefore, the intercept with the y-axis of the linear fits in Fig. 3b can be considered as a good estimate for $\sigma^2_{V,inj,hydro}$, assuming this contribution is independent of the injection volume. Fig. 4a represents the resulting volumetric contribution to band broadening ($\sigma^2_{V,inj.vol}$) when this value is, according to Eq. (3), subtracted from the total $\sigma^2_{V,inj}$ for the different cases given in Fig. 3a. It is clear that an almost perfect overlap is found for small V_{inj} (and also for larger V_{inj} when using the same needle seat). This agreement was expected, as this part of the variance only represents the effect of the injection volume which, for the same volume, should be independent of the flow effects in any subsequent tubing located before the detector. For volumes larger than 2µL, a slightly higher contribution was found for the 75µm compared to the 120µm needle seat capillary. It is still unclear where

this (unexpected) observation comes from, as the overlap is almost perfect for lower volumes. This observation was maintained over an extensive set of repeated experiments (results not shown). The larger dispersion for the 75µm capillary for large injection volumes is however of little practical relevance as it is anyhow of little use to employ a low dispersion needle seat capillary in combination with such large injection volume.

Also added to Fig. 4a are the observed peak variances (corrected for offset) on System 2, i.e. an Infinity 1290 system which had a standard needle injector (i.e. without sample loop pre-compression). The slightly higher observed values are however due to the pressure dip that occurs due to recompression of the sample loop upon injection, which causes a slightly lower flow rate during a brief moment right after the injection. Since the sample peak elutes for a large part during this period, it passes slower through the detector (and hence with a larger peak width in time) than expected based on the nominal flow rate. When compensating for this effect, by calculating the actual flow rate at each point using the difference in pressure, a very good agreement of $\sigma^2_{V,inj.vol}$ for both injectors was found (data not shown). This discrepancy between observed and actual peak variance contribution is important to consider whenever performing any extra-column band broadening study with flow-through needle injectors without sample loop pre-compression. In any case where the sample peak elutes during the injection pressure dip (which almost always occurs when replacing the column by zero dead volume union), the actual flow rate in the detector cell is different (lower) that the set value F_{set} and hence the observed time based peak variance σ_t^2 is no longer related to σ_V^2 by $\sigma_V^2 = \sigma_t^2 \cdot F_{set}^2$.

The most important observation from Fig. 4a however is that Eq. (4), suggesting a linear relation variation between $\sigma^2_{V,inj,vol}$ and V_{inj}^2, is certainly not valid over the entire range of injection volumes. Moreover, the initial slope of the curve (slope≅1) shows that the value of the proportionality constant for the small V_{inj} typically used in UHPLC (say $V_{inj} \leq 2\mu L$) is much larger than assumed in the largest body of literature, proposing a range of $1/8 < 1/\theta_{inj} < 1/5$.

The evolution of the proportionality constant is illustrated in Fig. 4b, showing how the values of θ_{inj} derived from the $\sigma^2_{V,inj,vol}$-values reported in Fig. 4a rather assume a constant value of around $\theta_{inj} \cong 1.1$ in the small injection volume range (V_{inj} < 1.25 µL). For the larger volumes (V_{inj} >2.5µL), this value becomes larger, apparently tending towards a value of θ_{inj} equal to ≅ 7 to 8, i.e., getting relatively close to the theoretical maximum of 12 (=perfectly rectangular band without dispersion). Rather than being a constant, the θ_{inj}-value in the range of 2-10µL clearly follows a trend that can be described by (see full line curves in Fig. 4b):

$$\theta_{inj} = \frac{b_{inj} \cdot V_{inj}^2}{a_{inj} b_{inj} + V_{inj}^2} \qquad (V_{inj} > 2\mu L) \qquad (5a)$$

Introducing this into Eq. (4) we obtain:

$$\sigma^2_{V,inj.vol} = a_{inj} + \frac{V^2_{inj}}{b_{inj}} \quad (V_{inj}>2\mu L) \qquad (5b)$$

Wherein a_{inj} and b_{inj} are mere empirical fitting parameters.

For the 120µm capillary, $a_{inj} \cong 2.7\mu L^2$ was found while b_{inj} was equal to 10.2. For the 75µm seat capillary, the values correspond to 3.5µL² and 9.2 for a_{inj} and b_{inj} respectively. The fitting lines added to Fig. 4b show the two regimes: one for $V_{inj}<1.5\mu L$ where $\sigma^2_{V,inj.,vol}$ varies with V_{inj}^2 according to Eq. (2), with θ_{inj} equal to $\cong$ 1.1.; and one for $V_{inj}>2\mu L$ where $\sigma^2_{V,inj.,vol}$ varies according to Eq. (4b), also displaying a linear increase of $\sigma^2_{V,inj.vol}$, but now with a much smaller slope and a significant intercept on the y-axis. A qualitatively similar variation of θ_{inj} with injection volume was previously reported by Lauer and Rozing [17] short cutting the injector to the UV detector with a 4µL flow cell. In this case, the θ_{inj}-value remained close to 2 for an injection volume of 2-4µL and reached a plateau around 8-9 for V_{inj}=90 µL (see Fig. 3 in [17]). The increase in θ_{inj} was also reported by Claessens *et al.* [29].

The low θ_{inj}-values for the injection volumes typically encountered in UHPLC applications show that the injection volume itself can have a significant contribution to the extra-column effects, especially when working on systems with very small extra-column dispersion in the order of 1 to 5µL² [1,9-11,14,15,21,41,42]. For example, for an injection volume of 1µL, the contribution to band broadening coming from the sample plug itself would be estimated based on the values suggested in literature to be equal to about 0.125µL² (taking θ_{inj}=8), which is almost negligible, but is in fact close to 1µL² (θ_{inj}=1), which is 20% or more of the total system dispersion when using a flow-through needle injector on an optimized ultra-high performance LC instrument.

To understand the reasons behind these observed values, detailed numerical simulations of the injection process (sample load, transfer and elution from the needle) would have to be made (as were presented by Grinias *et al.* for a capillary system with a loop injector [3]), but this will require to know to the very last detail the actual geometry and hydrodynamic behavior. Further work is planned to investigate the injection process using computational fluid dynamic simulations in some simplified cases. From a physical perspective, it can however be expected that the band broadening originating from the sample introduction in the mobile phase stream is the result of the parabolic flow profile that is established when drawing the sample into the needle and, upon injection, eluting it in the opposite direction. This hydrodynamic dispersion can in turn be expected to be counteracted by radial diffusion during the sample load (typically at a flow rate around 100µl/min or 0.6s per µL sample volume) and during the movement of the needle from sample vial to the injector needle seat. In addition, for large injection volumes, the sample is no longer solely drawn into the needle, but also in the subsequent sample loop. As the internal volume of the needle is around 2.6µL, it can be expected that a part of the sample ends up in the loop for all volumes above 1.3µL (the latter value follows directly from the fact that the parabolic flow profile doubles the axial volume of a band). As the loop is a coiled piece of tubing, as opposed to the straight injection needle, and since it is well known that secondary flow effects enhance radial mixing in coiled vs. straight capillaries [30,43-47], this might also contribute to a difference in dispersion behavior for larger injection volumes.

3.3 Hydrodynamic contribution to band broadening for flow-through needle injector measured via on-tubing LIF

As illustrated in the previous paragraph, extrapolating $\sigma^2_{V,inj}$ vs. V_{inj}^2 towards zero allows to distinguish between injection volume ($\sigma_{V,inj.V}^2$) and the hydrodynamic contribution ($\sigma_{V,inj.hydro}^2$). As the dispersion in the tubing and valves is expected to depend on the mobile phase velocity, the experiments were repeated for four small injection volumes (0.25, 0.5, 0.75 and 1µL) at different flow rates (0.1-1.2mL/min). The results are given in Fig. 5a for the 75µm needle seat capillary on System 1, showing a gradual increase of $\sigma_{V,inj}^2$ with the flow rate, a trend which slowly flattens at the higher flow rates. By plotting (data not shown) $\sigma^2_{V,inj}$ as a function of V_{inj}^2 for each of the individual flow rates (i.e., by plotting the data for each flow rate according to the vertical arrow added to Fig. 5a) and extrapolating the linear fit to zero (following the same approach as was done for the 0.7mL/min flow rate case shown in Fig. 3b), we obtain the value of $\sigma^2_{V,inj.hydro}$ for each different value of F. The resulting values were plotted in Fig. 5b as a function of the flow rate (blue solid data). Injection volumes smaller than 0.25µL were not used for the linear fits because of the higher scatter due to the much smaller signal intensity and concomitantly lower signal-to-noise ratio (see discussion in previous paragraph).

The exercise was subsequently repeated for a 120µm needle seat capillary (red diamonds in Fig. 3b and 5b) on System 1. A quadratic fit curve (thin full line) was added to both data sets to guide the eye. For the 75µm tubing, $\sigma^2_{V,inj.hydro}$ initially increases steeply up to F=0.6 ml/min, after which it flattens off towards a constant value of around 0.6µL². Overlaid on the figure are the data obtained for an injection volume of 0.1µL (75µm tubing data set), i.e. for a case where the contribution due to the injection volume can be expected to be negligible (even when taking θ_{inj}=1, the volumetric contribution only accounts for 0.01µL²). Although the repeat experiments show a rather large scatter (as discussed early, see also the $\pm 2\sigma$ error bars), a good agreement of the average values was found with the data obtained *via* the extrapolation method, indicating that the latter provides a good estimate of the hydrodynamic contribution and that the two contributions are indeed close to additive as assumed in Eq. (3).

For the 120µm tubing, a similar trend with F was observed, but the dispersion here levels off to a much higher value of 1.2µL². This was expected as larger needle seat capillary ID tubing results in a larger dispersion contribution, whereas the rest of the system remains constant (rotor valve and stator, (sharp) turns, changes in ID…). The saturating trend observed in both cases is typical when investigating the band broadening in open-tubular systems such as the connection capillaries and valves used in chromatographic systems [7,18,48]. This trend can be well approximated by the following exact analytical solution, originally derived in [49] and rewritten in the present form in [23]:

$$\sigma^2_{V,tub} = \frac{\pi \cdot F \cdot d_{tub}^4 \cdot L_{tub}}{384 \cdot D_m} \cdot \left[1 - \frac{u_0 \cdot d_{tub}^2}{a \cdot D_m \cdot L} \cdot \left(1 - e^{-a \cdot D_m \cdot L_{tub} / (u_0 \cdot d_{tub}^2)} \right) \right] \quad (6)$$

with F the volumetric flow rate, d_{tub} the tubing diameter (75µm or 120µm), L the length of the tubing between needle seat and injector valve (15cm), D_m the molecular diffusion coefficient (taken as $1.2 \cdot 10^{-9} m^2/s$ [47]) and the geometrical parameter for pressure driven flow in a cylindrical tube a=60.18 [49], with $u_0 = 4 \cdot F/(d_{tub}^2 \cdot \pi)$. Note that the factor preceding the straight brackets is the classic, long time limit Taylor-Aris result. This is the regime prevailing at low flow rates. The expression between the brackets describes the transient effects at shorter times (i.e., at higher flow rates). It describes how the incomplete radial equilibration results in an almost constant contribution, independent of the flow rate, hence the leveling-off of the data in Fig. 5b at high velocities.

Comparing the data (dashed curves added to Fig. 5b) obtained via Eq. (6), it is however clear that the measured hydrodynamic dispersion originating from the injector was much larger than that expected from the injector seat capillary alone, as the measured values also include dispersion in the needle seat capillary, rotor valve and stator, (sharp) turns, changes in ID (needle to seat, capillary to valve port, valve port to rotor…), etc. . The capillary dispersion can be expected to be significantly smaller for the 75µm tubing than for the 120µm (due to the d_{tub}^4-dependency in Eq. 6), hence the difference between both dashed curves. The difference between the actual total dispersion and that predicted from the capillary by Eq. (6) was very similar for both the 75µm and the 120µm. This probably indicates that a significant (especially for the 75µm tubing) contribution to dispersion originates from the internal flow paths in the needle seat and the injector valve itself. These are the same for both needle seat capillaries.

3.4 Effect of injector volume for a flow-through needle injector measured via a post-column UV-detector

In the present study, we also wanted to include a flow-through needle injector from a different vendor (System 4). For practical reasons, these experiments could not be carried out using the LIF set-up used in the previous sections. Instead, we relied on the UV-detector signal recorded at the end of a complete system, i.e., with a column in place (avoiding elution during the pressure dip, see earlier). The total dispersion $\sigma_{V,tot}^2$ observed in a classical UV detector set-up for retained compounds, with a chromatographic column, is given by (rewriting Eq. 1 and using Eq. 3)

$$\sigma_{V,tot}^2 = \sigma_{V,inj.vol}^2 + \sigma_{V,inj.hydr}^2 + \sigma_{V,tubing}^2 + \sigma_{V,col}^2 + \sigma_{V,det}^2 \quad \text{with} \quad \sigma_{V,col}^2 = \frac{V_0^2}{N_{col}} \cdot (1+k)^2 \qquad (7)$$

If one is only interested in the contribution originating from the injection volume ($\sigma^2_{V,inj,vol}$), this remains accessible by measuring $\sigma_{V,tot}^2$ for different injection volumes, and extrapolating the plot of $\sigma_{V,tot}^2$ vs. V_{inj}^2 to the point where $V_{inj}^2=0$ to obtain the contribution for the last 4 terms in Eq. (7) (assuming no mass overloading occurs at high injection volumes). Subsequently subtracting this value from each of the $\sigma^2_{V,tot}$-values obtained for the different V_{inj}-cases, a plot of $\sigma_{V,inj.V}^2$ versus V_{inj}^2 can be obtained. These experiments were performed on a Acquity UPLC I-class system (very low dispersion system) under typical chromatographic conditions (50/50 v%/v% ACN/H_2O)

with methyl- and propylparaben as sample compounds and using a 2.1mmx100mm column packed with 2.5µm particles. Fig. S4 in the Supplementary Material shows how the $\sigma^2_{V,inj,vol}$-values (obtained by correcting for the extrapolated hydrodynamic and column contribution which is measured at V_{inj}=0) vary as a function of V_{inj}^2, which is the equivalent of Fig. 4a (but now for an injector from a different vendor), showing a very similar behavior. The corresponding values of θ_{inj} vs. V_{inj} are shown in Fig. 6, which is the equivalent of Fig. 4b. For injection volumes below 1µL, a lot of scatter was observed on the data, as the contribution to dispersion coming from the column and the rest of the chromatographic system (i.e. the "offset" at V_{inj}=0) was much larger (11 and 23µL² for methyl- and propylparaben respectively) than the one coming from the injection volume. For this method, a rather low retention factor was thus preferred, as otherwise the contribution to $\sigma_{V,tot}^2$ becomes too large (see Eq. 7). The same behavior and general trend was observed as for the LIF measurements on the other injector (Agilent), which was confirmed by performing the same measurements with column and UV detector on the Agilent system (see Fig. S5 in the Supplementary Material for a comparison of both systems), showing that similar values of $\sigma_{V,inj.vol}^2$ and θ_{inj} were obtained for both flow-through needle injectors.

3.5 Volumetric and hydrodynamic dispersion for fixed loop injections measured via on-tubing LIF

To investigate the effect of the injection volume in a fixed loop injector, four capillaries with an ID of 120µm and different lengths and two capillaries with an ID of 75µm and 170µm were used (see also Fig. 2b) as sample loops on System 3. To determine the actual volume of the capillaries, some injections were performed using the injector of Infinity II 1290 system at different volumes between 0.75µL and 5µL without changing the set-up described in Fig. 1b (as any shift in the optical window of the LIF can affect the signal response) to establish a calibration curve of peaks area vs. injection volume (R^2>0.9999, results not shown). This could then be used to determine the actual peak volumes when performing injections in the fixed loop mode. The different lengths and the nominal and actual loop volumes are given in Table 1. A possible explanation for the deviations between the nominal and actual loop volumes may be some errors on the measurement of the tubing length (sample loop is not a straight tube), and mainly the tolerance in the inner diameter of the stainless steel tubing. In addition, a sample loop with a nominal volume of 5µL was used which, based on the peak area, had an actual volume of 3.8µL. Based on the capillary length (~10cm), this corresponds to an actual inner diameter of 220µm.

Figure 7a plots the measured $\sigma^2_{V,inj}$-values as a function of the flow rate for the different loops using the set-up depicted in Fig, 1b. Please note the y-axis was broken to more clearly represent the wide range in variances. The first observation that can be made was that there was almost no effect of the flow rate on the observed volumetric variance for almost all loops (especially the 75 and 120µm tubing). The 170µm loop shows a slight increase (around 20% from 0.3 to 1ml/min). The only loop showing a significant flow rate dependency was the one with the 5µL nominal volume (3.8µL actual volume), for which a clear linear increase in variance with flow rate was observed (+70% for the 0.3-1ml/min range), showing that for very large ID loops, a significant flow rate dependency of the dispersion from the injection volume can be expected, as previously observed [18,38].

Focusing only on the smaller injection loop volumes, i.e., those depicted in the bottom part of Fig. 7a, we also compared them with the dispersion data measured for a 1µL injection in the flow-through needle (75µm needle seat capillary) put in overlay (see black crosses and black fit curve to guide the eye). Comparing this data set with the fixed loop injector having the same volume (i.e., comparing with the lowest data set of the fixed loops represented by the full circles and corresponding to almost the same 1.1µL injection volume), it is readily clear that the dispersion in the flow-through injector was much larger, especially at higher flow rates. In addition, the flow-through needle injector shows a clear dependency of the dispersion on the flow rate. This is in part due to the flow rate-dependent dispersion in the injection seat capillary (see Fig. 5), needle seat and valve ports, but also due to the flow rate dependency of the elution from the needle or loop, as it was also observed for the large ID fixed loop injectors.

Given the nearly absent flow rate dependency, Figure 7b plots the flow-rate average of the measured values of $\sigma^2_{V,inj}$ shown in Fig. 7a as a function of V_{inj}^2 for the 120µm ID loops (with error bars $\pm 1\sigma$ to represent the spread around the mean caused by the very slight variation with the flow rate as observed in Fig. 7a), as well as the minimum and maximum values for the other diameters. Fig. 7b can be considered as the equivalent of the type of plot shown in Fig. 4a, except that the entire variance was plotted here and not only the volumetric contribution, as done in Fig. 4a (because the hydrodynamic contribution is difficult to determine independently, see below). The data for the 120µm loops can be relatively well approximated with a linear fit (R^2=0.998), with an offset of 0.34µL² and a slope of 0.119. As such, this relationship can again be represented using the newly introduced expression (Eq. 4b) with a_{inj}=0.34µL² and b_{inj}=8.4. Comparing the a_{inj}-values, we can conclude the a_{inj}–value for fixed loop injectors is much smaller than for flow through needle injectors. As it was difficult to use sufficiently small injection volumes, the interpolated intercept of a_{inj}=0.34µL² might not include only $\sigma^2_{V,inj.vol}$, but also a small contribution from $\sigma^2_{V,inj.hydro}$ due to the dispersion in the injection valve. As a consequence, it was impossible to isolate the contribution from $\sigma^2_{V,inj.hydro}$ from the value of a_{inj}. The value of b_{inj} is close to the 'ideal' value of 12 for rectangular plug. The inevitable elution from the capillary, causing a steep front but shallow tail due to the parabolic flow profile, prevents the injection of an ideal rectangular plug. When only a part of the sample loop would be injected, in a so-called 'timed' or 'temporary"-injection mode [30,33,37,38], the tail can be cut off and an almost perfect rectangular plug can be injected. Giving the relative high flow rates in LC, this would require extremely fast switching (e.g. 100ms for a 1µL injection at 0.6ml/min), and, in addition, the accuracy and repeatability of the injection volume will be determined by the switch time and the stability of the flow rate during the injection. Unfortunately, practical constraints did not allow to implement smaller loops, because a minimum length in tubing is required to connect the two ports of the injector loop and because smaller ID loops gave rise to large pressure shocks upon injection.

For the larger ID loops (colored 170 and 220µm open data points in Fig. 7b), the $\sigma^2_{V,inj}$-value for the lowest flow rate is very close to that of the 120µm loop (black data and straight fitting line), in agreement with the fact the hydrodynamic dispersion in capillaries is smallest at low flow rates (see also Fig. 5b), but deviates significantly at

the highest flow rate. It can therefore be inferred that this strong increase is the result of the hydrodynamic dispersion experienced during the elution of the sample plug from the cylindrical loop. This dispersion is expected to increase with increasing flow rate and thus giving the largest deviation from the 120µm case at the highest from rate. For the 75µm loop, only a small variation (in fact decrease) in peak variance was observed over the investigated flow rate range. The decrease could be related to the relative large additional pressure drop upon injection when the 75µm ID, 22cm long loop is switched in the flow path that can cause a short increase in flow rate (and thus apparent narrower peaks).

4. Conclusions

The contribution from the injection to the extra-column band broadening in state-of-the-art UHPLC instrumentation was investigated using on-tubing fluorescence measurement of the sample plug shape directly after the injection valve. By extrapolating the experimental data to an infinitesimally small volume, it was possible to determine and distinguish the contribution that increases with increasing injection volume ($\sigma_{V,inj.vol}^2$) from the inevitable contribution ($\sigma_{V,inj.hydro}^2$) that remains even when a very small volume is injected for a flow-through needle injector and is caused by the hydrodynamic dispersion in the internal parts of the injector. Good agreement is found for the values of $\sigma_{V,inj.hydro}^2$ obtained through extrapolation and those observed when injection a very small sample volume of 0.1µL

For flow-through needle injectors, it was found that the values of $1/\theta_{inj}$ to be used in the expression for $\sigma_{V,inj.vol}^2$ ($\sigma_{V,inj.vol}^2=V_{inj}^2/\theta_{inj}$) were typically significantly larger than assumed in literature where values of 1/5-1/8 are suggested. For small injection volumes (<2µL), a value of $1/\theta_{inj}\approx0.8$-1 is a more accurate approximation, whereas for larger injection volumes this values decreases to a minimal value around $1/\theta_{inj}\approx1/8$ around V_{inj}=10µL. For the hydrodynamic contribution, a clear increase in dispersion with flow rate was found, reaching a plateau around 0.8ml/min of 0.6µL² or 1.2µL² for the 75µm and 120µm needle seat capillaries respectively, showing a clear advantage of the low dispersion injection needle for a set-up with minimized extra-column dispersion.

For a loop-type injector operated in a full loop mode, the increase in peak variance with V_{inj}^2 was much less pronounced with an apparent value for $1/\theta_{inj}\approx1/8$ over the entire range of investigated injection volumes of 1.1µL to 4.5µL when using 120µm or narrower ID loops. The total injector variance was found to be $\sigma^2_{V,inj}=$ 0.34µL²+0.12.V_{inj}^2 when using 120µm or narrower ID loops. The offset of 0.34µL² includes both a contribution from $\sigma^2_{V,inj.vol}$, but also from $\sigma^2_{V,inj.hydro}$ due to the dispersion in the injection valve. Little or no variation of peak variance with flow rate was observed for both 75µm and 120µm ID loops. For larger ID sample loops, a clear increase of peak variance with flow rate was observed (+20% for 170µm and +70% for 220µm ID loops). Given the larger $\sigma^2_{V,inj}$ values for wider loops, it is best recommended to use a narrow ID loop within the practical limitations of pressure drop as this increases with ~$1/ID^6$ for a fixed loop volume. From an extra-column dispersion perspective, the fixed loop injector yields smaller peak volumes (lower $\sigma^2_{V,inj}$) than a flow through needle injector,

both in regards hydrodynamic dispersion due to the lack of needle seat and needle seat capillary and due to a smaller injection volume dependency ($1/\theta$ is smaller ~ 1/8), especially for small injection volumes. In practice, however, many other aspects, such as required sample volume (larger for fixed loop), accuracy, precision and carry-over (fixed loop requires an additional cleaning step) also influence a practitioners' choice of injector type.

Acknowledgements:

K.B. acknowledges a Research Grant from FWO Vlaanderen (1520115N). M. van Wingerden (Waters, Zellik, Belgium) is kindly acknowledged for the gift of the chromatographic column. Monika Dittmann (Agilent Technologies, Waldbronn, Germany) is kindly acknowledged for the gift of the 75µm ID needle seat capillary needle seat.

References

[1] S. Fekete, I. Kohler, S. Rudaz, D. Guillarme, Importance of instrumentation for fast liquid chromatography in pharmaceutical analysis, J. Pharm. Biomed. Anal. 87 (2014) 105-119.

[2] R. De Pauw, K. Shoyket (Choiket), G. Desmet, K. Broeckhoven, Understanding and diminishing the extra-column band broadening effects in supercritical fluid chromatography, J. Chromatogr. A 1403 (2015) 132-137.

[3] J.P. Grinias, B. Bunner, M. Gilar, J.W. Jorgenson, Measurement and modeling of extra-column effects due to injection and connections in capillary liquid chromatography, Chromatogr. 2 (2015) 669-690.

[4] N. Lambert, S. Miyazaki, M. Ohira, N. Tanaka, A. Fellinger, Comparison of the kinetic performance of different columns for fast liquid chromatography, emphasizing the contributions of column end structure, J. Chromatogr. A 1473 (2016) 99-108.

[5] Y. Vanderheyden, K. Broeckhoven, G. Desmet, Peak deconvolution to correctly assess the band broadening of chromatographic columns, J. Chromatogr. A 1465 (2016) 126-142.

[6] Y. Vanderheyden, K. Vanderlinden, K. Broeckhoven, G. Desmet, Problems involving the determination of the column-only band broadening in columns producing narrow and tailed peaks, J. Chromatogr. A 1440 (2016) 74-84.

[7] K.J. Fountain, U.D. Neue, E.S. Grumbach, D.M. Diehl, Effects of extra-column band spreading, liquid chromatography system operating pressure, and column temperature on the performance of sub-2-µm porous particles, J. Chromatogr. A 1216 (2009) 5979-5988.

[8] F. Gritti, G. Guiochon, On the extra-column band-broadening contributions of modern, very high pressure liquid chromatographs using 2.1 mm I.D. columns packed with sub-2 µm particles, J. Chromatogr. A 1217 (2010) 7677-7689.

[9] F. Gritti, G. Guiochon, On the minimization of the band-broadening contributions of a modern, very high pressure liquid chromatography, J. Chromatogr. A 1218 (2011) 4632–4648.

[10] F. Gritti, C.A. Sanchez, T. Farkas, G. Guiochon, Achieving the full performance of highly efficient columns by optimizing conventional benchmark high-performance liquid chromatography instruments, J. Chromatogr. A 1217 (2010) 3000-3012.

[11] D.V. McCalley, Instrumental considerations for the effective operation of short, highly efficient fused-core columns. Investigation of performance at high flow rates and elevated temperatures, J. Chromatogr. A 1217 (2010) 4561-4567.

[12] F. Gritti, N. Tanaka, G. Guiochon, Comparison of the fast gradient performance of new prototype silica monolithic columns and columns packed with fully porous and core–shell particles, J. Chromatogr. A 1236 (2012) 28-41.

[13] D. Spaggiari, S. Fekete, P.J. Eugster, J.-L. Veuthey, L. Geiser, S. Rudaz, D. Guillarme, Contribution of various types of liquid chromatography–mass spectrometry instruments to band broadening in fast analysis, J. Chromatogr. A 1310 (2013) 45-55.

[14] S. Fekete, D. Guillarme, Kinetic evaluation of new generation of column packed with 1.3 µm core–shell particles, J. Chromatogr. A 1308 (2013) 104-113.

[15] F. Gritti, S.J. Shiner, J.N. Fairchild, G. Guiochon, Evaluation of the kinetic performance of new prototype 2.1 mm x 100 mm narrow-bore columns packed with 1.6 µm superficially porous particles, J. Chromatogr. A 1334 (2014) 30-43.

[16] S. Buckenmaier, C.A. Miller, T. van de Goor, M.M. Dittmann, Instrument contributions to resolution and sensitivity in ultra-high performance liquid chromatography using small bore columns: Comparison of diode array and triple quadrupole mass spectrometry detection, J. Chromatogr. A 1377 (2015) 64-74.

[17] H.H. Lauer, G.P. Rozing, The selection of optimum condition in HPLC I. The Determination of External Band Spreading in LC Instruments, Chromatographia 14 (1981) 641–647.

[18] K.W. Freebairn, J.H. Knox, Dispersion measurements on conventional and miniaturized HPLC systems, Chromatographia 19 (1984) 37-47.

[19] H.A. Claessens, C.A. Cramers, M.A.J. Kuyken, Estimation of the Band Broadening Contributions of HPLC Equipment of Column Elution Profiles, Chromatographia 23 (1987) 189-194.

[20] A.G.-G. Perrenoud, C. Hamman, M. Goel, J.-L. Veuthey, D. Guillarme, S. Fekete, Maximizing kinetic performance in supercritical fluid chromatography using state-of-the-art instruments, J. Chromatogr. A 1314 (2013) 288-297.

[21] F. Gritti, G. Guiochon, Accurate measurements of the true column efficiency and of the instrument band broadening contributions in the presence of a chromatographic column, J. Chromatogr. A 1327 (2014) 49-56.

[22] N. Lambert, A. Fellinger, Performance of the same column in supercritical fluid chromatography and in liquid chromatography, J. Chromatogr. A 1409 (2015) 234-240.

[23] K. Vanderlinden, K. Broeckhoven, Y. Vanderheyden, G. Desmet, Effect of pre- and post-column band broadening on the performance of high-speed chromatography columns under isocratic and gradient conditions, J. Chromatogr. A 1442 (2016) 73-82.

[24] G. Kahsay, K. Broeckhoven, E. Adams, G. Desmet, D. Cabooter, Kinetic performance comparison of fully and superficially porous particles with a particle size of 5 mm: Intrinsic evaluation and application to the impurity analysis of griseofulvin, Talanta 122 (2014) 122-129.

[25] D.R. Stoll, X. Li, X. Wang, P.W. Carr, S.E.G. Porter, S.C. Rutan, Fast, comprehensive two-dimensional liquid chromatography, J. Chromatogr. A 1168 (2007) 3-43.

[26] P.J. Schoenmakers, G. Vivó-Truyols, W.M.C. Decrop, A protocol for designing comprehensive two-dimensional liquid chromatography separation systems, J. Chromatogr. A 1120 (2006) 282-290.

[27] M.J.E. Golay, J.G. Atwood, Early phases of the dispersion of a sample injected in Poiseuille flow, J. Chromatogr. 186 (1979) 353-370.

[28] J.G. Atwood, M.J.E. Golay, Dispersion of peaks by short straight open tubes in liquid chromatography systems, J. Chromatogr. 218 (1981) 79-122.

[29] H.A. Claessens, A. Burcinova, P. Mussche, C.C.E. van Tilburg, C.A.M.G. Cramers, Evaluation of injection systems for open tubular liquid chromatography, J. Microcolumn Sep. 2(3) (1990) 132-137.

[30] B. Coq, G. Cretier, J.L. Rocca, M. Porthault, Open or packed sampling loops in liquid chromatography, J. Chromatogr. Sci. 19 (1981) 1-12.

[31] A.C. Sanchez, J.A. Anspach, T. Farkas, Performance optimizing injection sequence for minimizing injection band broadening contributions in high efficiency liquid chromatographic separations, J. Chromatogr. A 1228 (2012) 338-348.

[32] B.L. Karger, M. Martin, G. Guiochon, Role of column parameters and injection volume on detection limits in liquid chromatography, Anal. Chem. 46 (1974) 1640-1647.

[33] A. Prüß, C. Kempter, J. Gysler, T. Jira, Extracolumn band broadening in capillary liquid chromatography, J. Chromatogr. A 1016 (2003) 129–141.

[34] M. Martin, C. Eon, G. Guiochon, Study of the pertinency of pressure in liquid chromatography II. Problems in equipment design, J. Chromatogr. 108 (1975) 229-241.

[35] J.J. Kirkland, W.W. Yau, H.J. Stoklosa, C.H. Dilks, Jr., Sampling and extra-column effects in high-performance liquid chromatography; influence of peak skew on plate count calculations, J. Chromatogr. Sci. 15 (1977) 303-316.

[36] K.P. Hupe, R.J. Jonker, G. Rozing, Determination of band-spreading effects in high-performance liquid chromatographic instruments, J. Chromatogr. 285 (1984) 253-265.

[37] S.R. Bakalyar, C. Phipps, B. Spruce, K. Olsen, Choosing sample volume to achieve maximum detection sensitivity and resolution with high-performance liquid chromatography columns of 1.0, 2.0 and 4.6 mm I.D., J. Chromatogr. A 762 (1997) 167-185.

[38] M.D. Foster, M.A. Arnold, J.A. Nichols, S.R. Bakalyar, Performance of experimental sample injectors for high-performance liquid chromatography microcolumns, J. Chromatogr. A 869 (2000) 231–241.

[39] J. De Vos, K. Broeckhoven, S. Eeltink, Advances in Ultrahigh-Pressure Liquid Chromatography Technology and System Design, Anal. Chem. 88 (2016) 262-278.

[40] U.S. Raikar, C.G. Renuka, Y.F. Nadaf, B.G. Mulimani, A.M. Karguppikar, M.K. Soudagar, Solvent effects on the absorption and fluorescence spectra of coumarins 6 and 7 molecules: Determination of ground and excited state dipole moment, Spectrochimica Acta Part A: Molecular and Biomolecular Spectroscopy 65 (2006) 673-677.

[41] J.O. Omamogho, J.P. Hanrahan, J. Tobin, J.D. Glennon, Structural variation of solid core and thickness of porous shell of 1.7 mum core–shell silica particles on chromatographic performance: narrow bore columns, J. Chromatogr. A 1218 (2011) 1942–1953.

[42] S. Fekete, J.L. Veuthey, D.V. McCalley, D. Guillarme, The effect of pressure and mobile phase velocity on the retention properties of small analytes and large biomolecules in ultra-high pressure liquid chromatography, J. Chromatogr. A 1270 (2012) 127–138.

[43] A.K. Wong, B.J. McCoy, R.G. Carbonell, Theory of capillary chromatography: Effect of coiling and interphase mass transfer, J. Chromatogr. 129 (1976) 1-18.

[45] R. Tijssen, R.T. Wittebrood, Effect of column-coiling on the dispersion of solutes in gas chromatography, Part II: generalized theory, Chromatographia 5 (1972) 286-295.

[46] J.G. Atwood, J. Goldstein, Measurements of diffusion coefficients in liquids at atmospheric and elevated pressure by the chromatographic broadening technique, J. Phys. Chem. 88 (1984) 1875–1885.

[46] L.A.M. Janssen, Axial dispersion in laminar flow, Chem. Eng. Sci. 31 (1976) 215–218.

603 [47] H. Song, Y. Vanderheyden, E. Adams, G. Desmet, D. Cabooter, Extensive Database of Liquid Phase
604 Diffusion Coefficients of Some Frequently Used Test Molecules in RPLC and HILIC, J. Chromatogr. A 1455
605 (2016) 102–112.

606 [48] F. Gritti, T. McDonald, M. Gilar, Accurate measurement of dispersion data through short and narrow tubes
607 used in very high-pressure liquid chromatography, J. Chromatogr. A, 1410 (2015) 118–128.

608 [49] K. Broeckhoven, G. Desmet, Efficiency gain limits of the parallel segmented inlet and outlet flow concept in
609 analytical liquid chromatography columns suffering from radial transcolumn packing density gradients, J.
610 Chromatogr. A, 1258 (2012) 66-75.

611

Figure Captions

Figure 1: Schematic representation of the measurement set-up and the flow trajectory in **(a)** the flow-through needle injector and **(b)** the fixed loop injector. The flow path of the sample contributing to $\sigma^2_{V,inj}$ as defined in the present study is indicated by the dashed arrow.

Figure 2: Experimentally measured elution profiles directly after the injector valve for **(a)** the flow-through needle injector with the 75µm needle seat capillary (System 1) and **(b-c)** for the fixed loop injector (System 3); (b) Four different loops with the same ID of 120µm but varying lengths of 8cm, 12cm, 22cm and 28cm; (c) loops with different ID and lengths (75µm-22cm, 170µm-9cm and 220µm-10cm) (full lines) and an overlaid comparison with two 120µm ID loops (12cm and 28cm) (dashed curves with color corresponding to the loop with the same volume).

Figure 3: Volumetric variance ($\sigma_{V^2,inj}$) of the injection peak as a function of the square of injection volume measured after the valve of the flow-through needle injector on System 1 **(a)** measured on a 50µm ID fused silica capillary 8cm after the valve for the case of a 75µm (blue circles) and a 120µm (red diamonds) ID needle seat capillary and measured on a 200µm ID capillary 80cm after the valve; **(b)** same data as (a) but zoomed-in on the low injection volume range. Dashed lines added to visualize the linear behavior. The dashed lines represent the equilibrium contribution $V_{inj}^2/12$, corresponding to the case where the injector would be able to produce a perfectly rectangular band.

Figure 4: (a) Volumetric contribution ($\sigma_{V^2,inj.vol}$) of the total injection peak variance data shown in Fig. 3 as a function of the square of injection volume. Same symbols as in Fig. 3. Green crosses represent the dispersion measured on a single needle injector without correction for the pressure dip during injection (System 2); The dashed line represents the equilibrium contribution $V_{inj}^2/12$, corresponding to the case where the injector would be able to produce a perfectly rectangular band. **(b)** θ_{inj}-values corresponding to the data represented in (a) and calculated according to Eq. (4). Fit curve (full line) calculated according to Eq. (5).

Figure 5: (a) Volumetric variance ($\sigma_{V^2,inj}$) of the injection peak as measured after the valve of the flow-through needle injector (System 1) as a function of flow rate for an injection volume of 0.25µL (green squares), 0.5µL (red diamonds), 0.75µL (black triangles) and 1µL (blue circles) for the 75µm ID needle seat capillary. **(b)** Volumetric peak variance of the hydrodynamic injector dispersion ($\sigma_{V^2,inj.hydro}$) contribution to the data shown in (a) as a function of flow rate for the 75µm (blue circles) and 120µm (red diamonds) ID needle seat capillary. Full lines represent the best quadratic fit to the data to guide the eye. Dashed lines represent the transient Taylor-Aris dispersion calculated according to Eq. (6). Experimental data for injection volumes of 0.1µL (75µm tubing data set) with $\pm 2\sigma$ error bars (open blue circles) are added for comparison.

Figure 6: θ_{inj}-values corresponding to the volumetric contribution ($\sigma_{V^2,inj.vol}$) of the total injection peak variance as a function of the injection volume, calculated according to Eqs. (4) and (7), measured on an Acquity I-class

instrument using a standard UV-detector with methyl- (red squares) or propylparaben (black triangles) as sample compound on a Xbridge BEH C18 2.5µm 2.1x100mm XP column with a 50/50 v%/v% ACN/H_2O mobile phase. The variation of $\sigma_{V^2,inj.vol.}$ with V_{inj}^2 is presented in Fig. S4 in the Supplementary Material.

Figure 7: (a) Volumetric variance ($\sigma_{V^2,inj}$) of the injection peak as a function of the flow rate for full loop injections with different sample loop volumes; full black symbols: 120µm ID loops with a length of 8cm (circles), 12cm (triangles), 22cm (squares) and 28cm (diamonds); open symbols: 75µm ID, 22cm (red diamonds), 170µm ID, 9cm (blue circles), 220µm ID, 10cm (green squares). Overlaid (black crosses) is the dispersion in the flow-through needle injector shown in Fig. 5a for the case of 1µL injection volume. **(b)** Plot of $\sigma_{V^2,inj}$ as a function of the square of the injection volume (same symbols as (a)). For the 120µm ID loops, the average of $\sigma_{V^2,inj}$-values measured at the different flow rates is plotted, with the errors bars representing $\pm$ one standard deviation of the slight variation around the mean caused by the very slight flow rate dependency as observed in (a). For the other loops, the values at the highest and lowest flow rates are plotted. The dashed line represents the equilibrium contribution $V_{inj}^2/12$, corresponding to the case where the injector would be able to produce a perfectly rectangular band.

Figure 1:

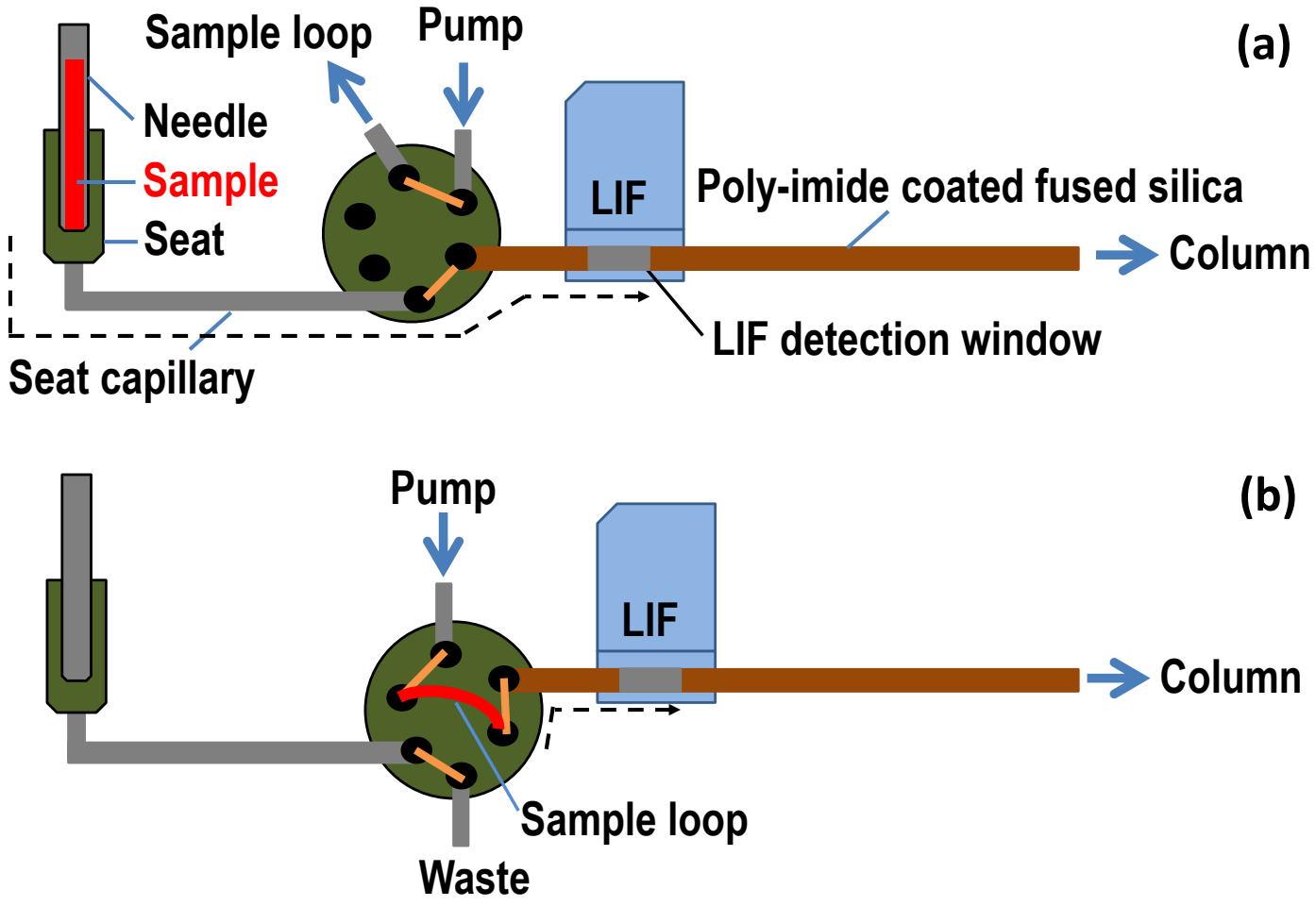
Sample loop
Pump
(a)
Needle
Sample
Seat
LIF
Poly-imide coated fused silica
Column
LIF detection window
Seat capillary
Pump
(b)
LIF
Column
Sample loop
Waste

Figure 2:

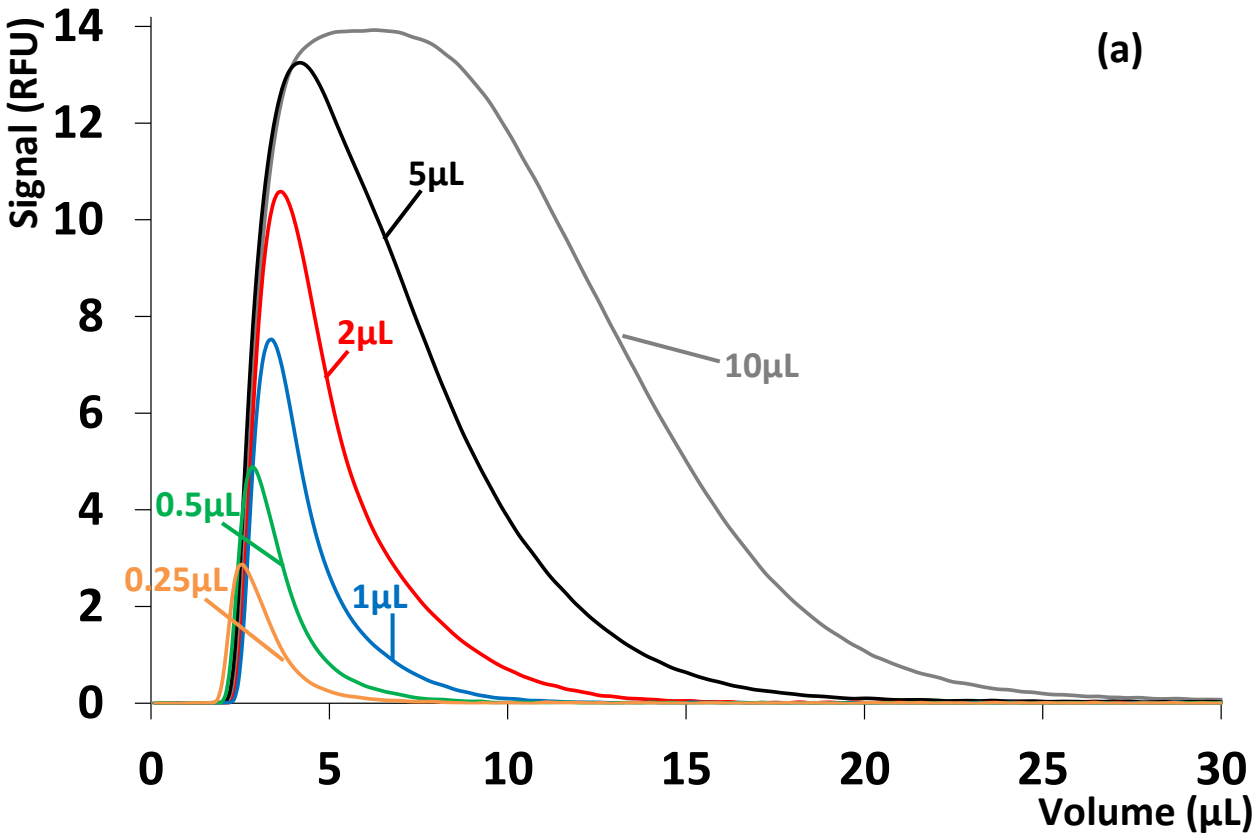
(a)
Signal (RFU)
14
12
10
8
6
4
2
0
0
5
10
15
20
25
30
Volume (µL)
5µL
2µL
10µL
0.5µL
0.25µL
1µL

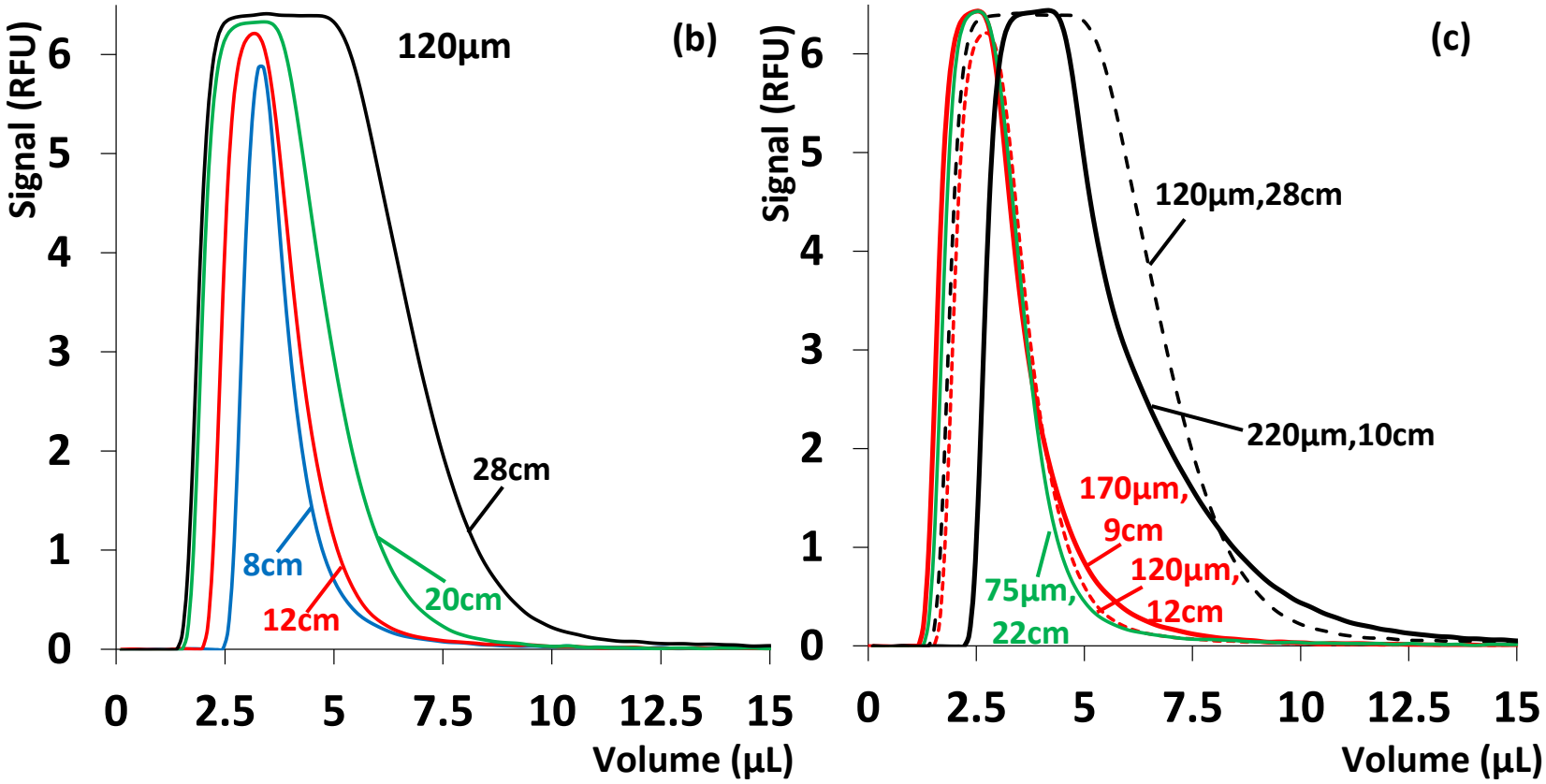
Signal (RFU)
120µm
(b)
28cm
8cm
12cm
20cm
0
1
2
3
4
5
6
0
2.5
5
7.5
10
12.5
15
Volume (µL)
Signal (RFU)
(c)
120µm,28cm
220µm,10cm
170µm,
9cm
120µm,
12cm
75µm,
22cm
Volume (µL)

Figure 3:

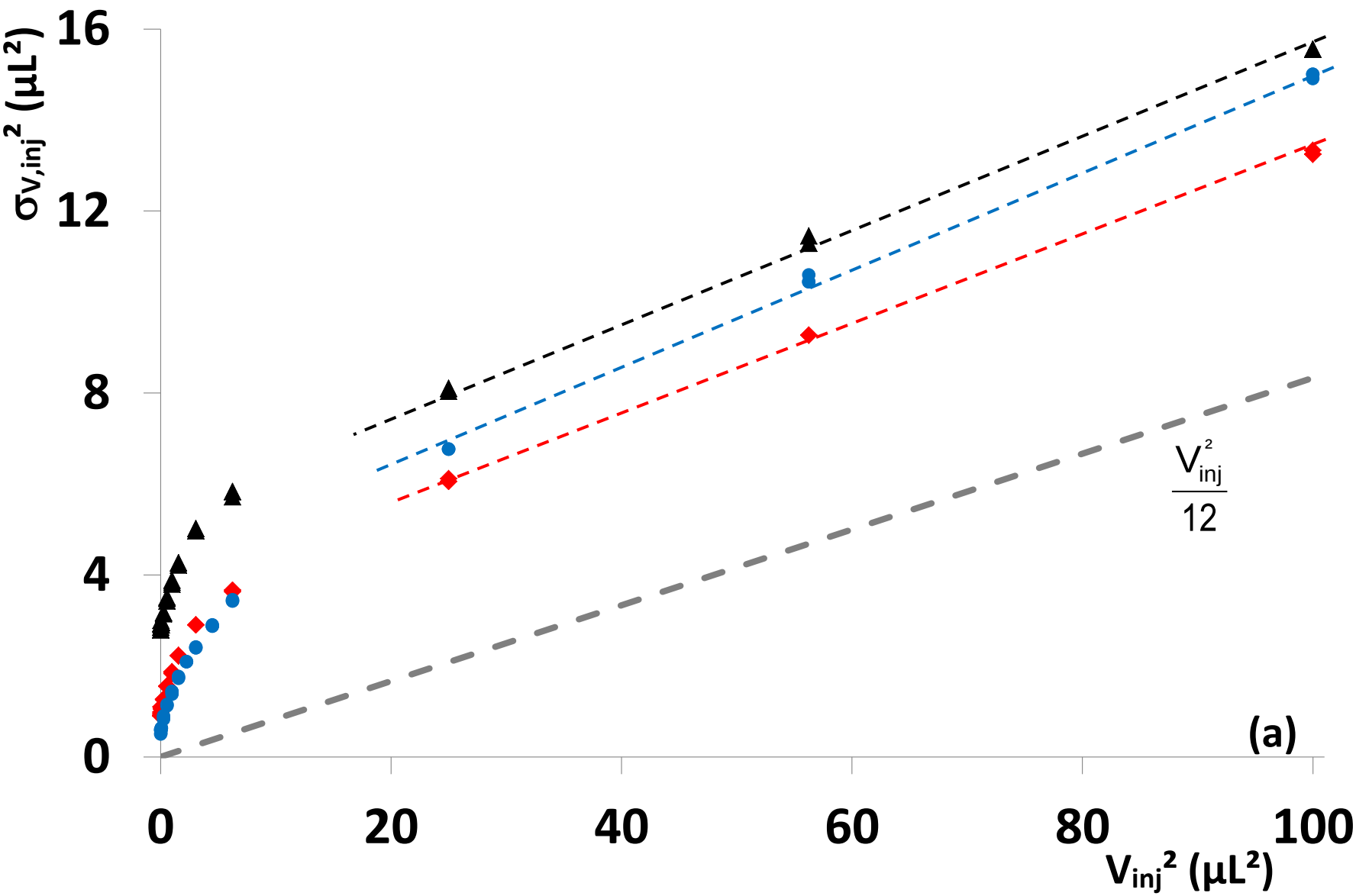
16
12
8
4
0
$\sigma_{V,inj}^2$ (µL²)
0
20
40
60
80
100
V_{inj}^2 (µL²)
$\frac{V_{inj}^2}{12}$
(a)

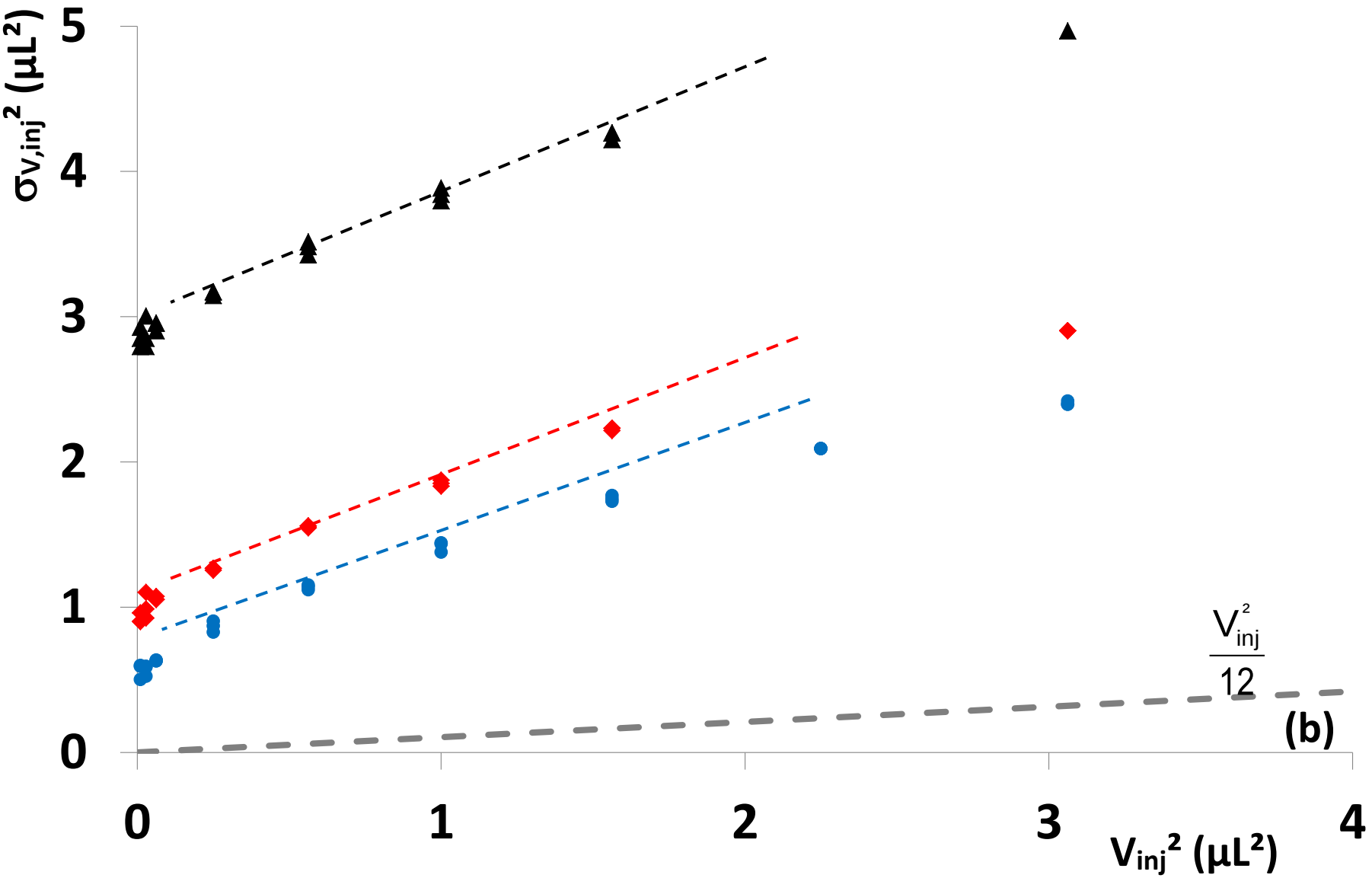
$\sigma_{V,inj}^2$ (µL²)
5
4
3
2
1
0
0
1
2
3
4
V_{inj}^2 (µL²)
$\frac{V_{inj}^2}{12}$
(b)

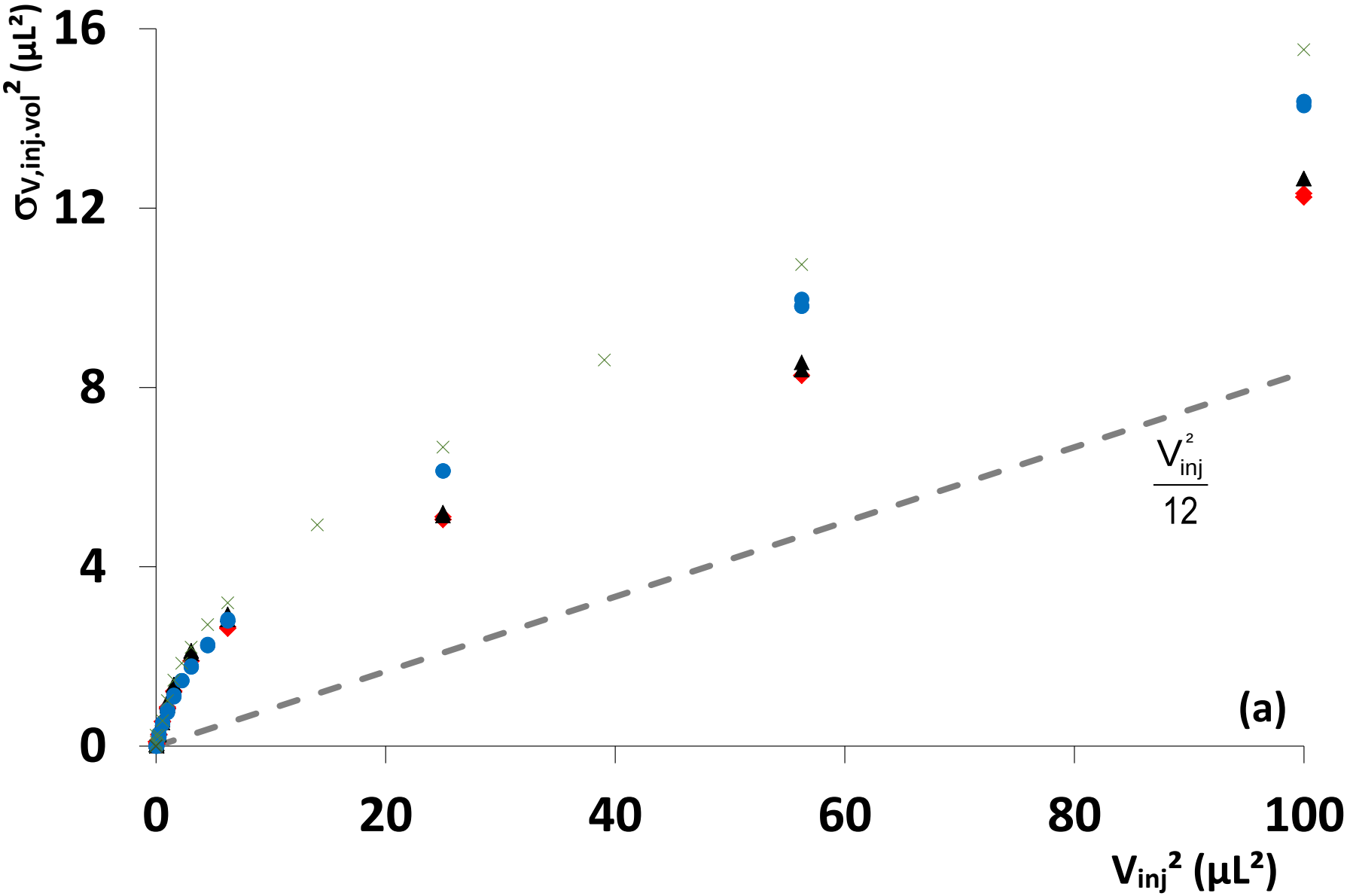
$\sigma_{V,inj.vol}^2$ (µL²)
16
12
8
4
0
0
20
40
60
80
100
V_{inj}^2 (µL²)
$\frac{V_{inj}^2}{12}$
(a)

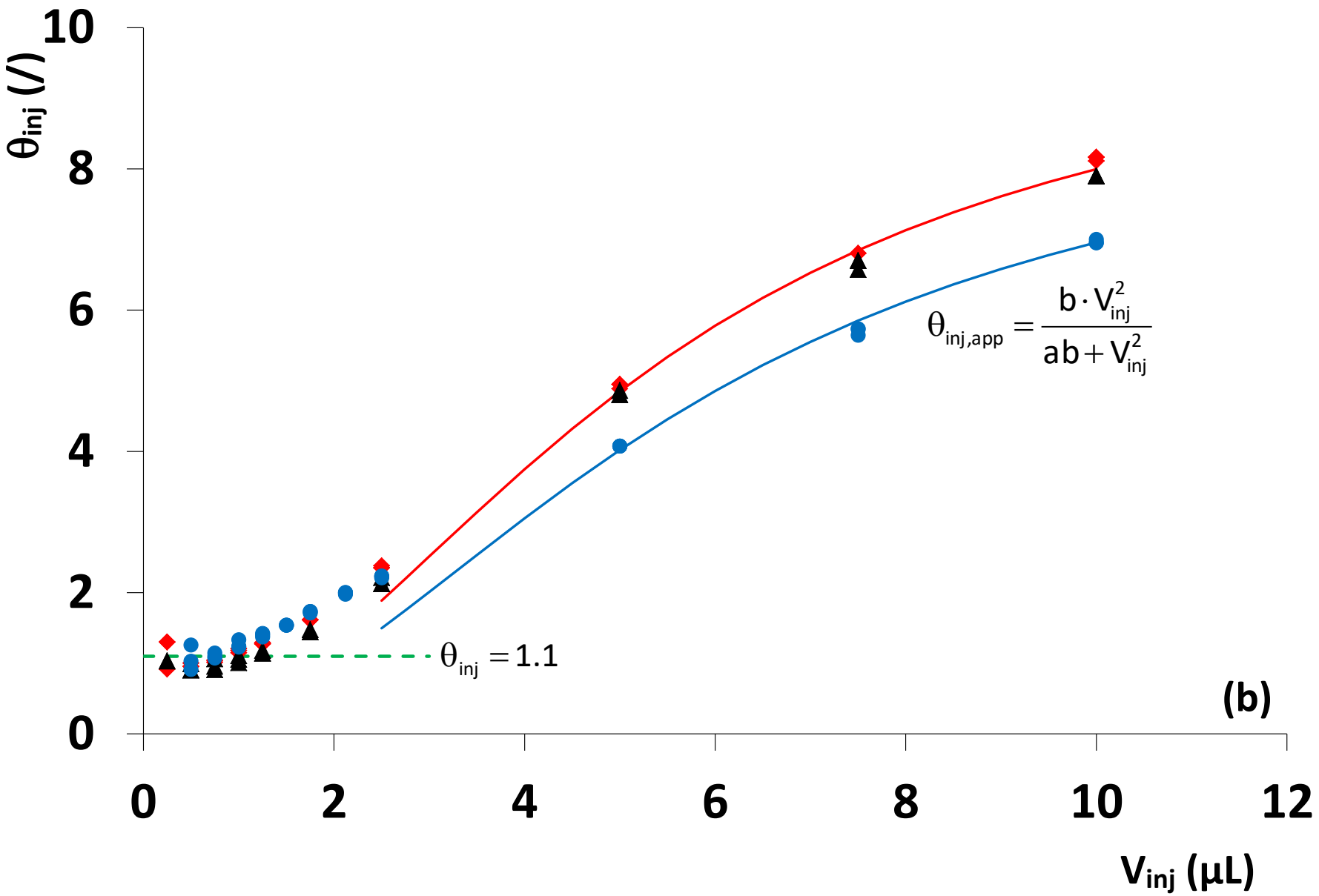
θinj (/)
10
8
6
4
2
0
0
2
4
6
8
10
12
Vinj (µL)
θinj,app = b·V²inj / ab + V²inj
θinj = 1.1
(b)

Figure 5

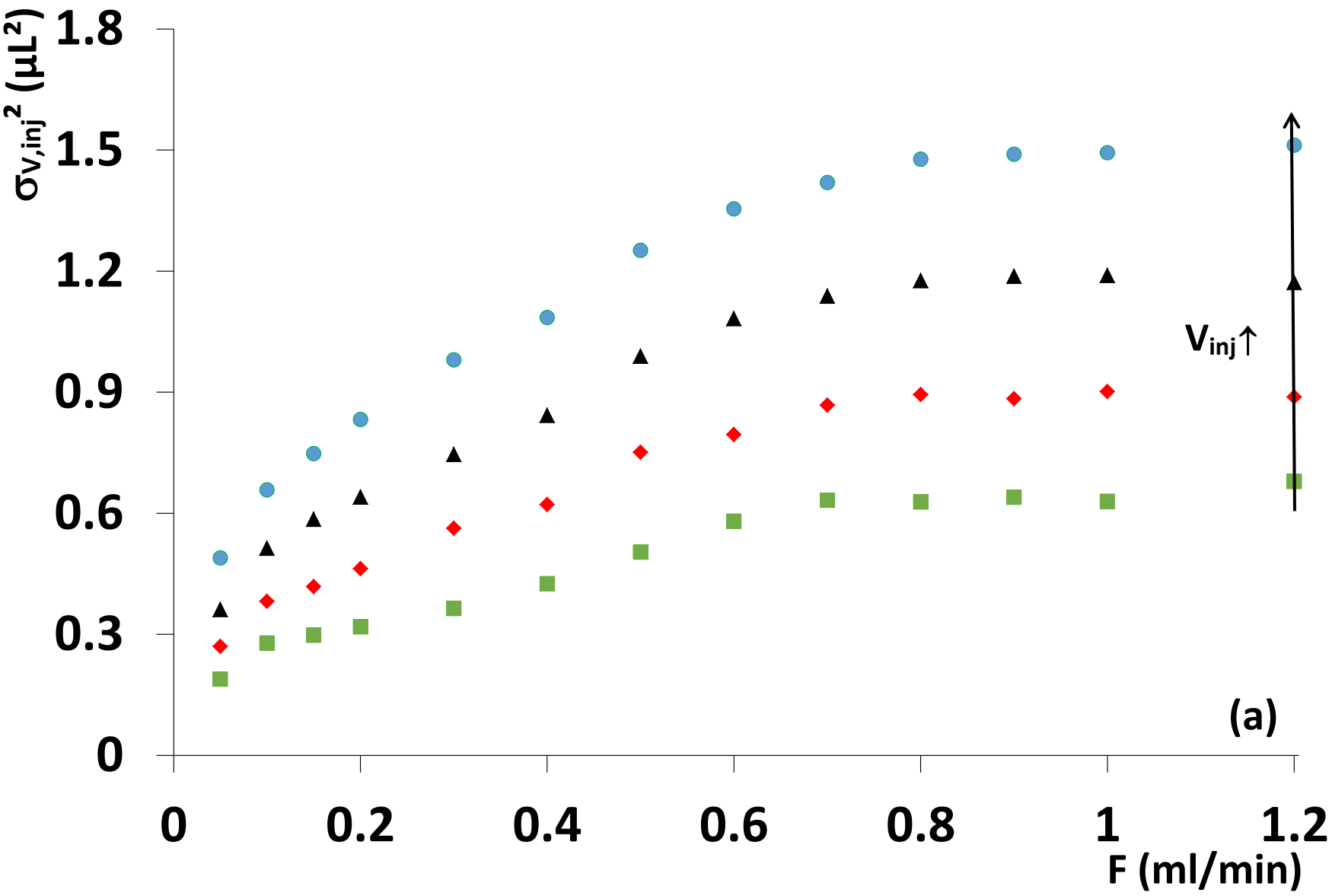

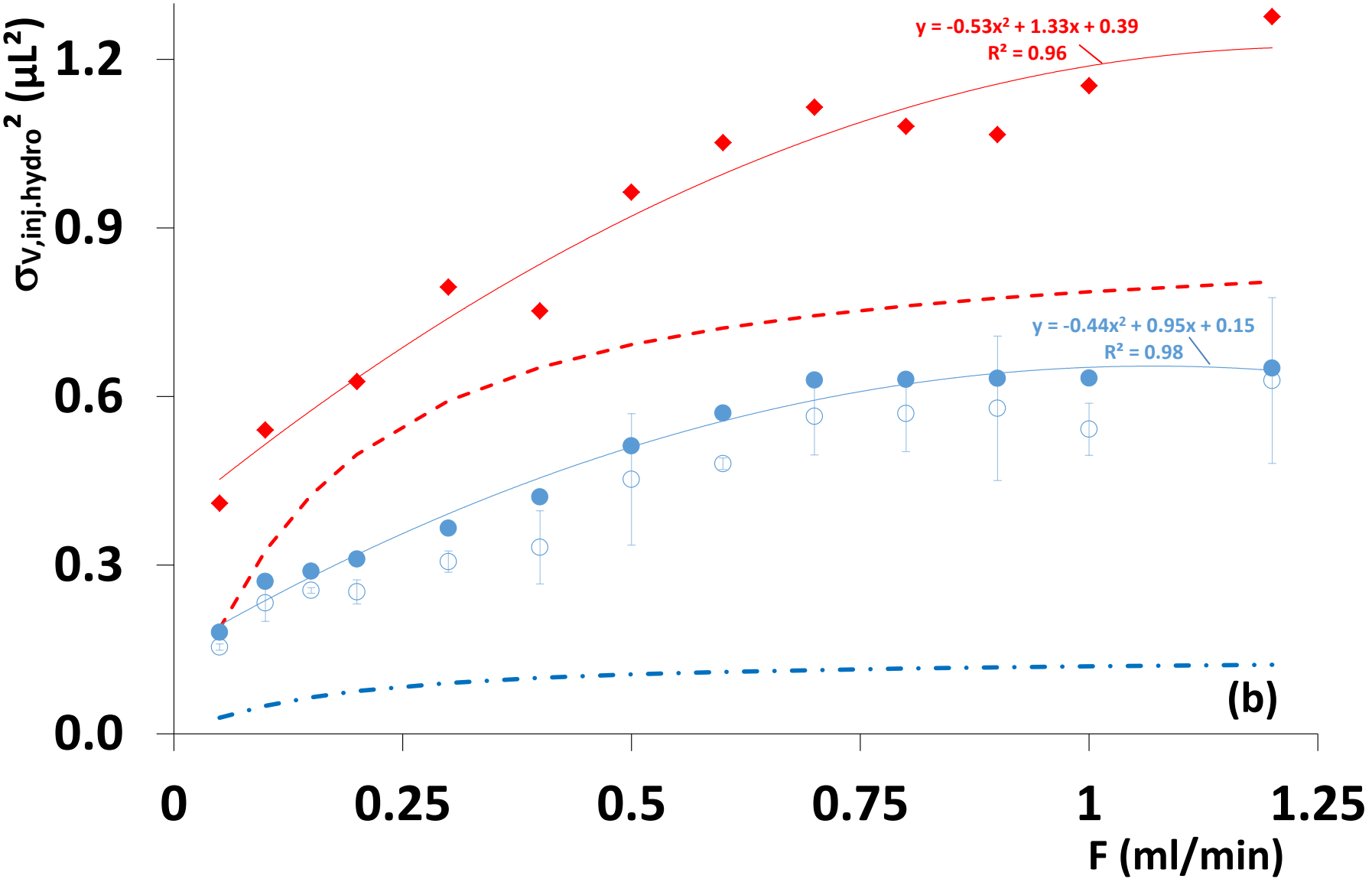
y = -0.53x² + 1.33x + 0.39
R² = 0.96
y = -0.44x² + 0.95x + 0.15
R² = 0.98
(b)
σV,inj.hydro² (µL²)
1.2
0.9
0.6
0.3
0.0
0
0.25
0.5
0.75
1
1.25
F (ml/min)

Figure 6:

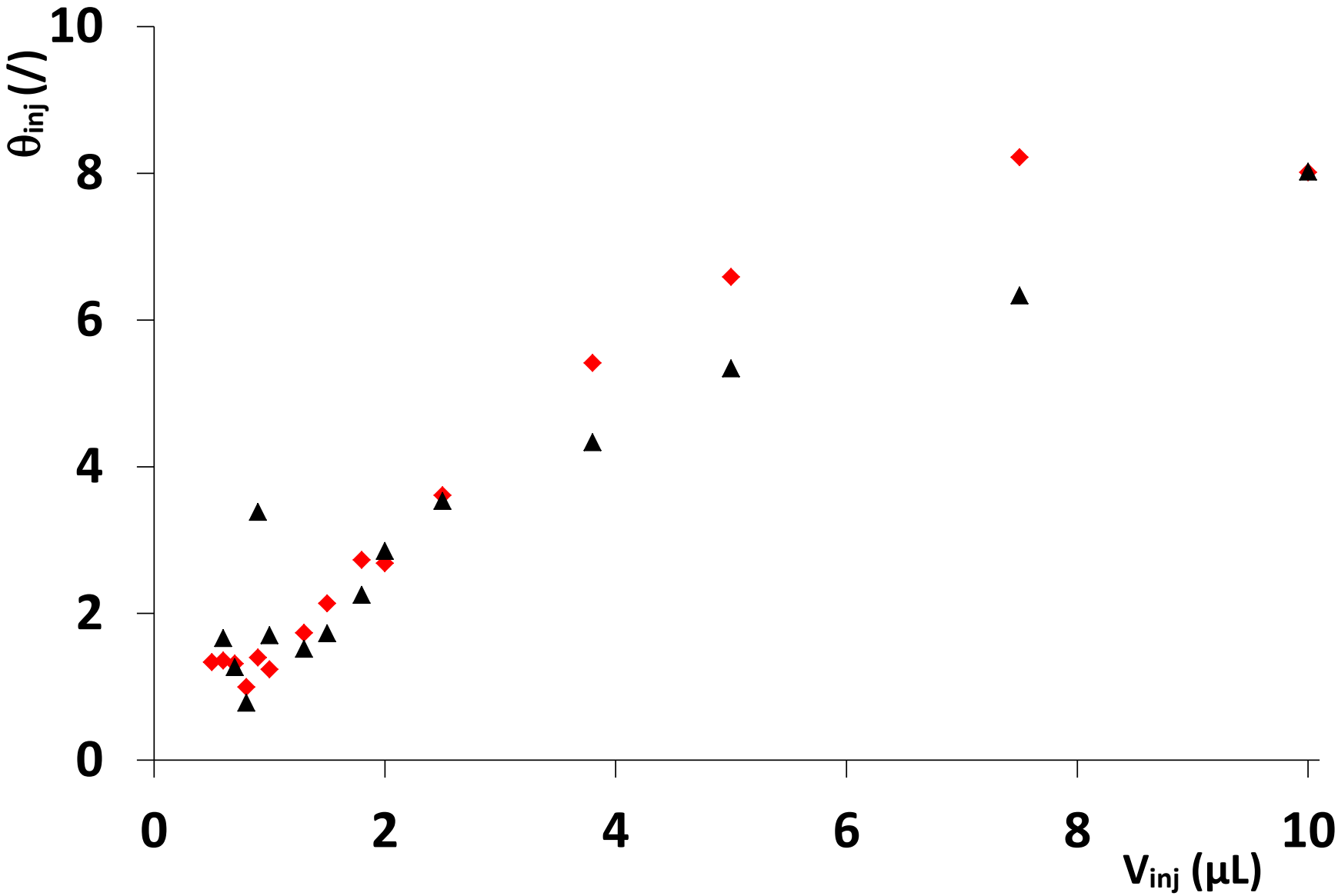

Figure 7

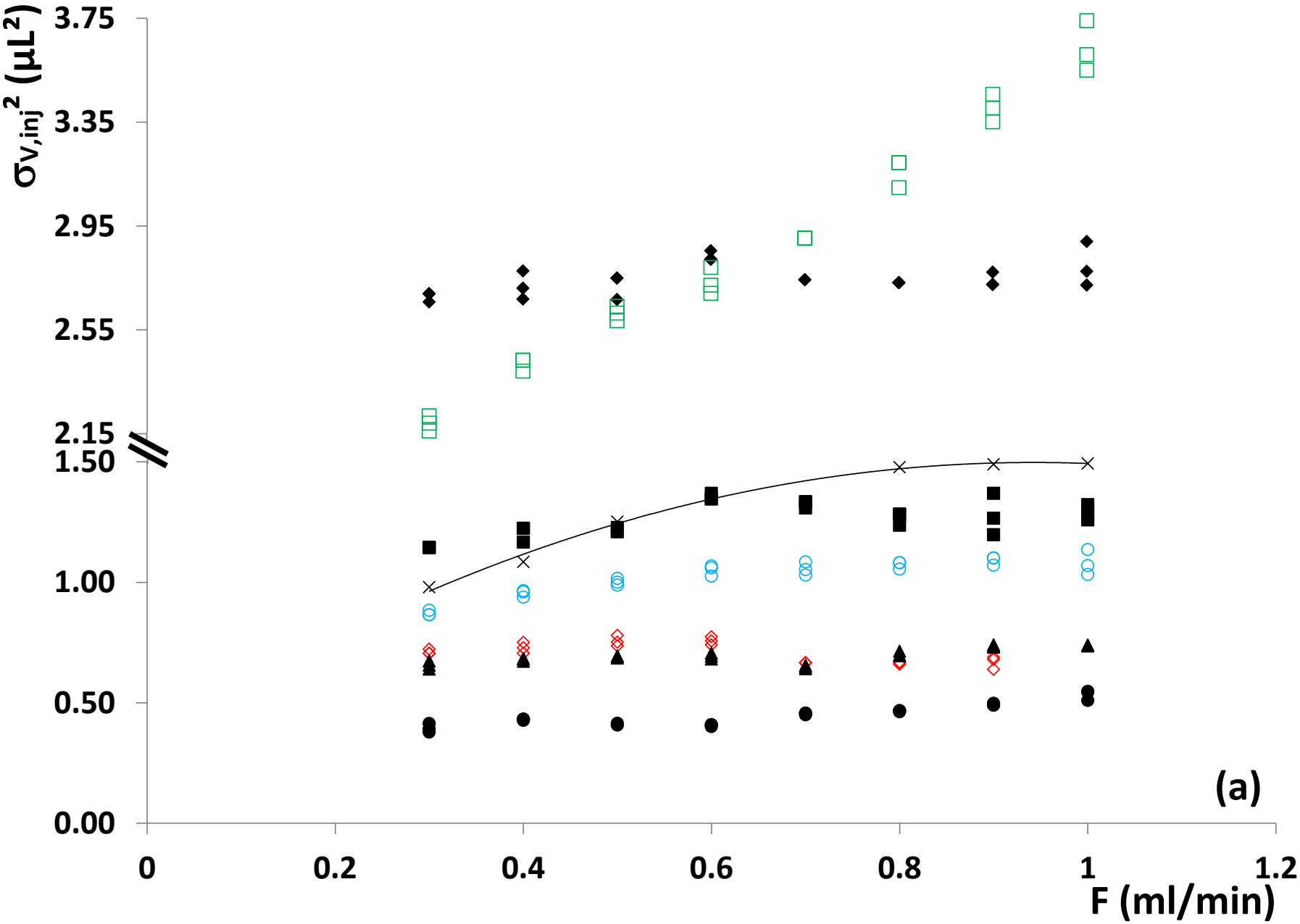
$\sigma_{V,inj}^2$ (µL²)
3.75
3.35
2.95
2.55
2.15
1.50
1.00
0.50
0.00
0
0.2
0.4
0.6
0.8
1
1.2
F (ml/min)
(a)

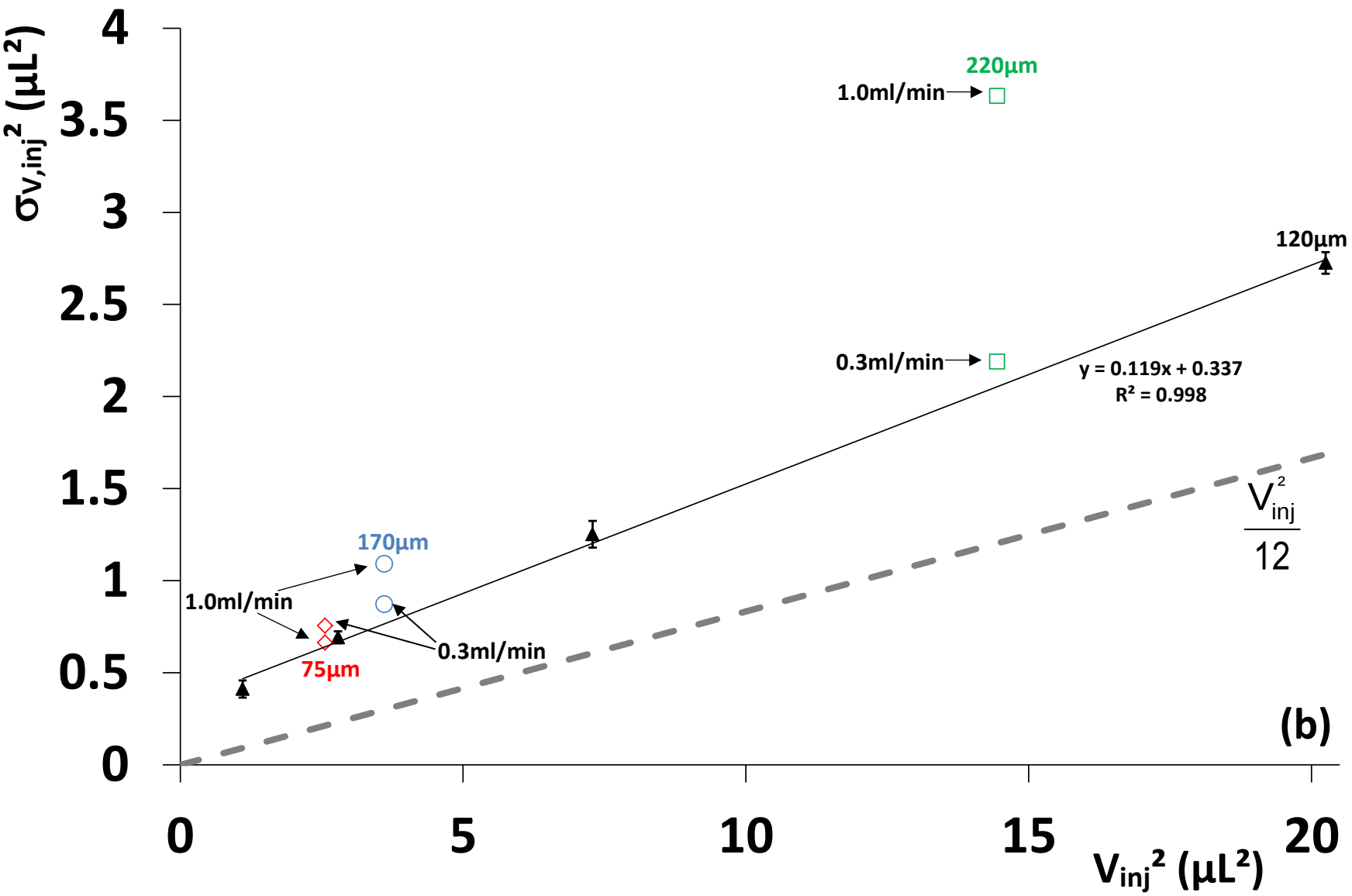
$\sigma_{V,inj}^2$ (µL²)
4
3.5
3
2.5
2
1.5
1
0.5
0
0
5
10
15
20
V_{inj}^2 (µL²)
220µm
1.0ml/min
120µm
0.3ml/min
y = 0.119x + 0.337
R² = 0.998
$\frac{V_{inj}^2}{12}$
170µm
1.0ml/min
0.3ml/min
75µm
(b)

Table 1: Geometrical parameters of the different loop capillaries used for the fixed loop injection mode and their nominal and actually measured volume

d_{tub} (µm)	Length (cm)	Actual Volume (µL)	Nominal volume (µL)
120	8	1.1	0.90
	12	1.7	1.4
	20	2.7	2.3
	28	4.5	3.2
170	9	2.0	2.3
75	22	1.6	1.0
220 ('5µL' loop)	10	3.8	5

Supplementary Material

On-tubing fluorescence measurements of the volumetric and hydrodynamic contribution to band broadening of contemporary injectors in high-performance liquid chromatography

Ken Broeckhoven[1,*], Kim Vanderlinden[1], Davy Guillarme[2], Gert Desmet[1]

[1] Department of Chemical Engineering, Vrije Universiteit Brussel, Pleinlaan 2, 1050 Brussels, Belgium

[2] School of Pharmaceutical Sciences, University of Geneva, University of Lausanne, CMU - Rue Michel Servet 1, 1211 Geneva 4, Switzerland

*Corresponding author: Phone: (+)32.(0)2.629.37.81, Fax: (+)32.(0)2.629.32.48, e-mail: kbroeckh@vub.ac.be

Abstract

Section 1 of the supplementary materials revisits the most important results from the main article, but now with the data analysis performed using the method of moments (vs. the 5σ-peak width method) to determine the peak variances, by discussing Figures 4, 5b and 7b. Section 2 shows the data for $\sigma_{V,inj.vol}^2$ measured using the UV detector with a column in place and a comparison of the obtained θ-values using this method on the Waters I-Class and Agilent Infinity II systems.

Section 1: Data Analysis using the method of moments

Fig. S1a shows a very similar evolution of $\sigma_{V,inj.vol}^2$ vs. V_{inj}^2 as Figure 4 where the 5σ-peak width method was used, but with slightly higher values (up to 16µL² in Fig. S1a vs. 12µL² in Fig. 4) and more scatter on the data. When translating these into θ_{inj}-values (Fig. S1b), it is found that for low injection volumes (<1µL) θ_{inj}-values around 0.4-1 are found, increasing up to a value around 6 for an injection volume of 10µL. These higher $\sigma_{V,inj.vol}^2$ and resulting lower θ_{inj} are the result of a very shallow tail exhibited by the peak profiles that has a larger influence in the method of moments calculation [9].

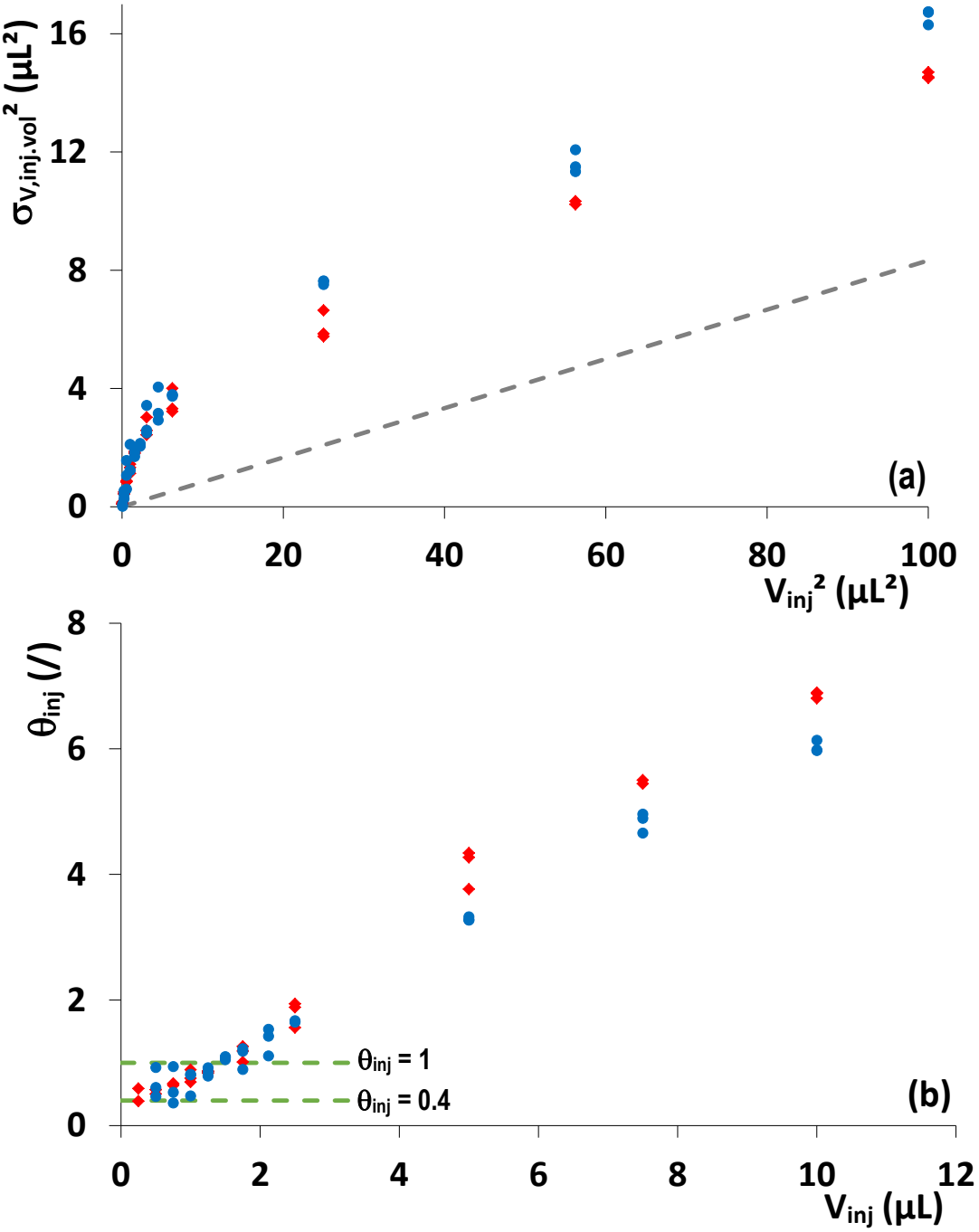

Figure S1: (a) *Volumetric contribution ($\sigma_{V,inj.vol}^2$) of the total injection peak variance as a function of the square of injection volume for a flow through needle injector, measured on a 50µm ID fused silica capillary 8cm after the valve for the case of a 75µm (blue circles) and a 120µm (red diamonds) ID needle seat capillary* ***(b)*** *θ_{inj}-values corresponding to the data represented in (a) and calculated according to Eq. (4).*

Fig. S2 shows a very similar evolution of $\sigma_{V,inj.hydro}^2$ vs. flow rate determined using the method of moments as Figure 5b where the 5σ-peak width method was used. The obtained values are once again higher (up to 1.5 and 0.9µL² in Fig. S2 vs. 1.2 and 0.6µL² in Fig. 5b) due to the strong influence of the shallow peak tail on the obtained peak variances using the method of moments. Once again, the difficulty in determining the peak integration boundary results in more scatter on the data, as clearly visible on the overlaid results for 0.1µL injection volumes [9].

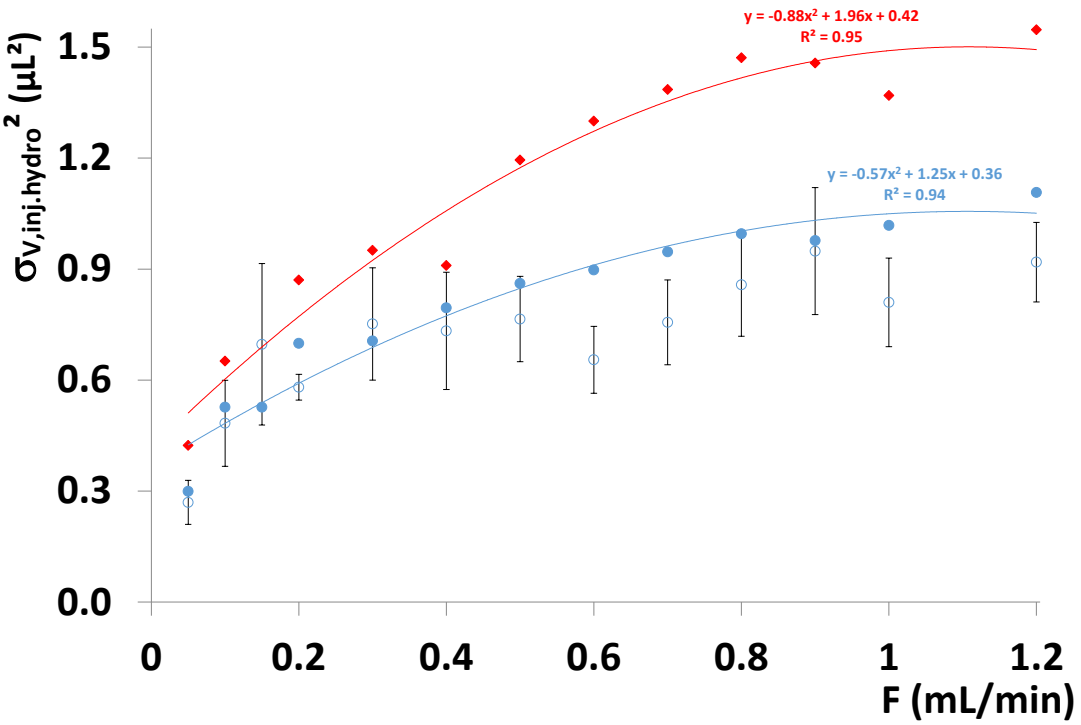

Figure S2: *Volumetric peak variance of the hydrodynamic injector dispersion ($\sigma_{V,inj.hydro}^2$) contribution as a function of flow rate for the 75µm (blue circles) and 120µm (red diamonds) ID needle seat capillary (flow through needle injector). Full lines represent the best quadratic fit to the data to guide the eye. Experimental data for injection volumes of 0.1µL (75µm tubing data set) with ±σ error bars (open blue circles) are added for comparison.*

Fig. S3 plots $\sigma_{V,inj}^{\ 2}$ vs. $V_{inj}^{\ 2}$ using the method of moments, similar to Fig. 7b where the 5σ-peak width method was used. For the 120µm ID loops, a linear increase of $\sigma_{V,inj}^{\ 2}$ with $V_{inj}^{\ 2}$ is found, although the data for the 20cm long loop shows some deviation from the linear trend. The inverse slope (b_{inj}) is however much less steep with a value of 4.3 vs. 8.4 when the 5σ-peak width is used. Again, the long shallow tails have a large influence on the obtained peak variances. The 220µm loop shows a similar behavior as in Fig. 7b, with a strong effect of flow rate on peak variance. Whereas the peak variance of the 170µm loop is in line with the trend of the 120µm ID loops, the 75µm loop exhibits a much larger value. This is because for this loop, the elution profiles show an extremely shallow but very long tail, relative to the 120 or 170µm ID loops (see Fig. 2c). This is probably the result of the abrupt change in flow through diameter when going from the stator to the narrow loop capillary, resulting in some dead zones, as also discussed by Grinias *et al.* [4].

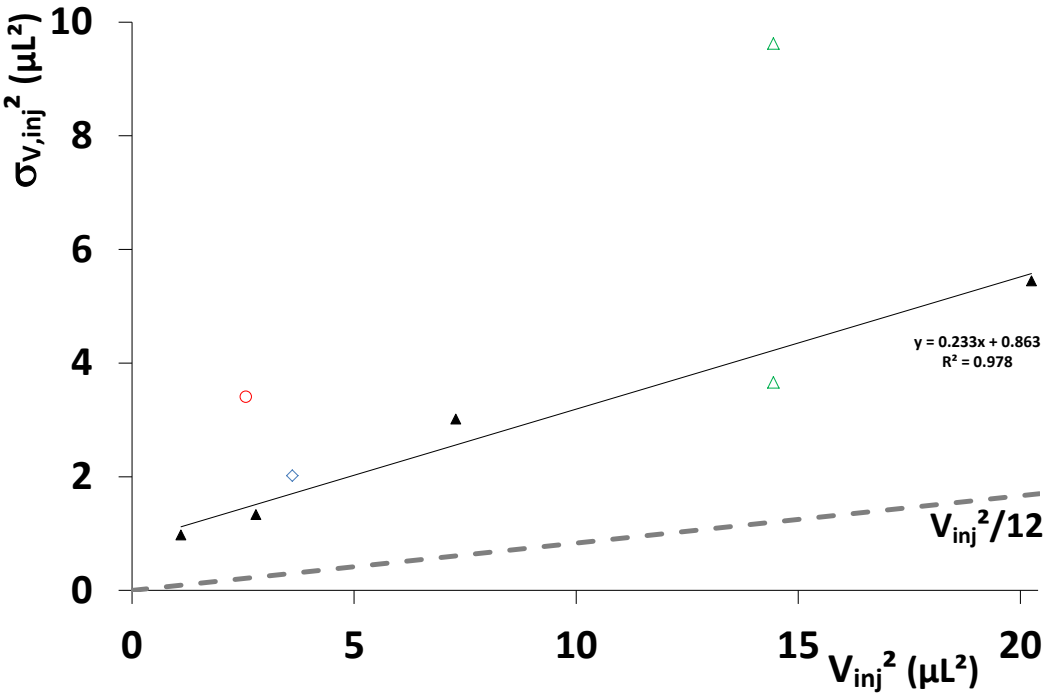

Figure S3: *Plot of $\sigma_{V,inj}^{\ 2}$ as a function of $V_{inj}^{\ 2}$ for a fixed loop injector in full loop mode. 120µm ID loops: full black triangles, 75µm loop: red circle, 170µm loop: blue diamond, 220µm loop: green triangle.*

Section 2: UV detector measurements

Fig. S4 plots $\sigma_{V,inj.vol.}^2$ vs. V_{inj}^2 measured using a UV detector and with a column in place, for two different compounds (methyl- and ethylparaben) at low retention factors to keep the column contribution as small as possible (see Eq. (7)). These values are obtained by correcting for the extrapolated hydrodynamic and column contribution which is measured at V_{inj}=0. Using Eq. (4), the corresponding θ_{inj}-values were determined (see Figs. 6 and S5).

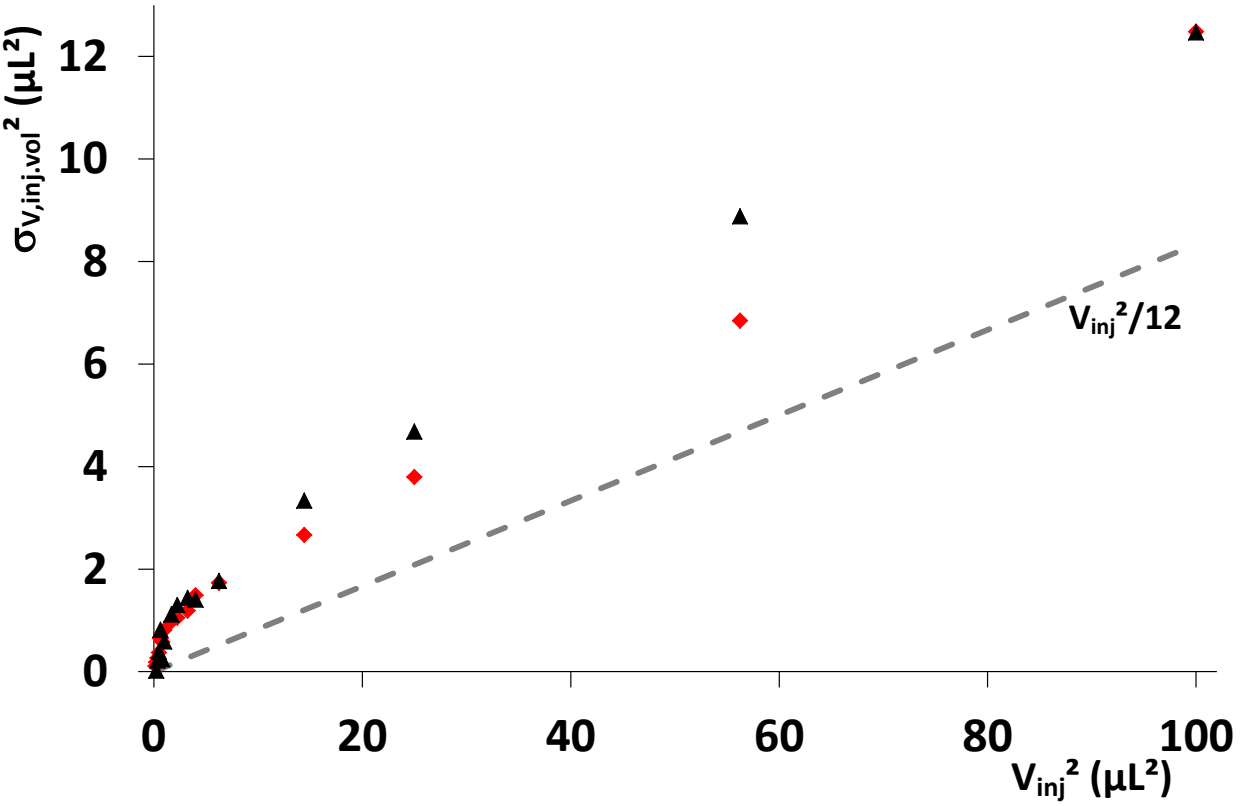

Figure S4: *Volumetric contribution ($\sigma_{V,inj.vol}^2$) of the total injection peak variance as a function of the square of injection volume measured on an Acquity I-class instrument using a standard UV-detector and methyl- (red squares) or propylparaben (black triangles) on a Xbridge BEH C18 2.5µm 2.1x100mm XP column with a 50/50 v%/v% ACN/H_2O mobile phase. The dashed line represents the equilibrium contribution $V_{inj}^2/12$, corresponding to the case where the injector would be able to produce a perfectly rectangular band.*

Fig. S5 shows a comparison of the θ_{inj}-values for propylparaben calculated using Eq. (4) on a Waters Acquity I-class instrument (same data as Fig. 6) and on an Agilent Infinity II system, using a standard UV-detector and a Xbridge BEH C18 2.5µm 2.1x100mm XP column with a 50/50 v%/v% ACN/H_2O mobile phase. A very similar trend is observed for both injectors, but the data obtained using the UV detector show significantly more scatter (not shown) than those measured using the LIF, especially for lower injection volumes. This is due to the fact that two large numbers ($\sigma_{v,tot}^2$ and $\sigma_{v,col}^2$) need to be subtracted in the UV detector case, which is not required for the LIF measurements.

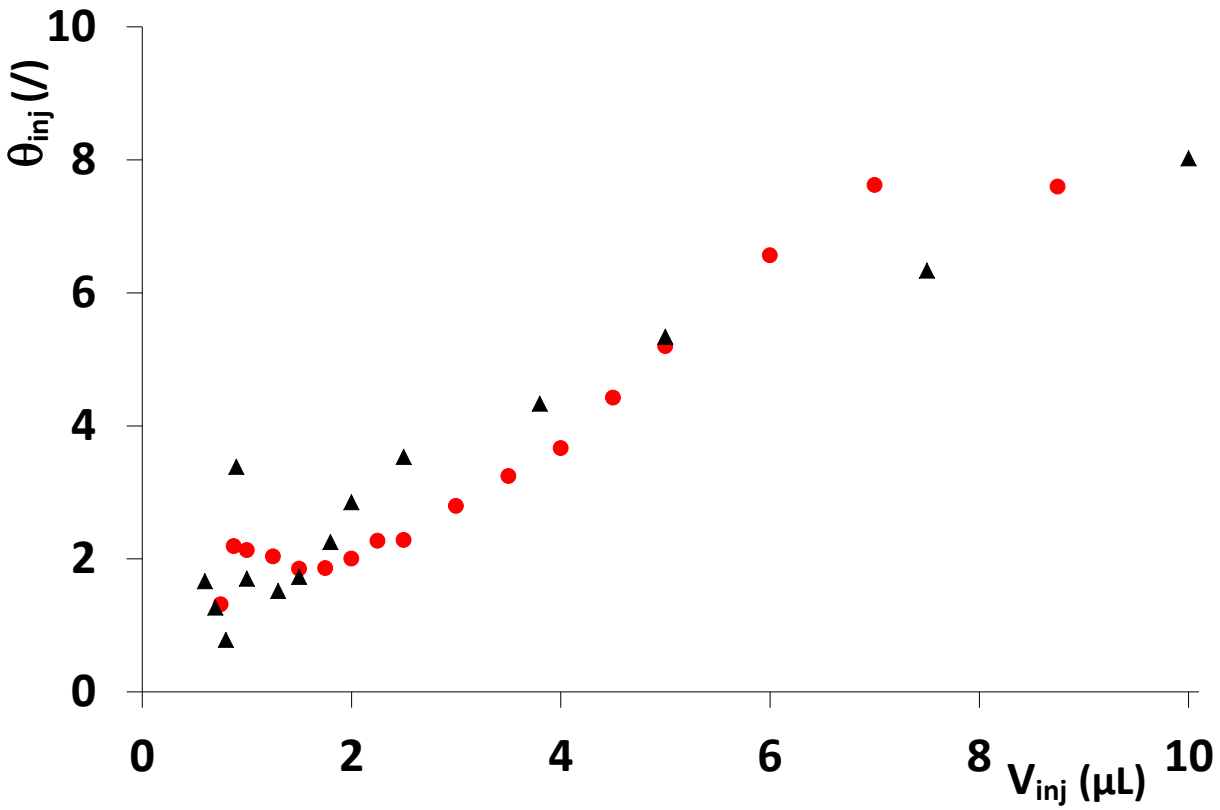

Figure S5: *Comparison of the θ_{inj}-values corresponding to the volumetric contribution ($\sigma_{V,inj.vol}^2$) of the total injection peak variance as a function of the injection volume, calculated according to Eqs. (4) and (7), measured using a standard UV-detector with propylparaben as sample compound on a Xbridge BEH C18 2.5µm 2.1x100mm XP column with a 50/50 v%/v% ACN/H_2O mobile phase on an Acquity I-class instrument (black triangles) and an Agilent Infinity II instrument (red circles).*